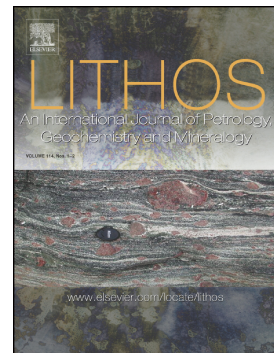


Accepted Manuscript

Evidence of sub-continental lithospheric mantle sources and open-system crystallization processes from in-situ U-Pb ages and Nd-Sr-Hf isotope geochemistry of the cretaceous ultramafic-alkaline-(carbonatite) intrusions from the Shillong Plateau, North-Eastern India



Rajesh K. Srivastava, Vincenza Guarino, Fu-Yuan Wu, Leone Melluso, Anup K. Sinha

PII: S0024-4937(19)30073-8

DOI: <https://doi.org/10.1016/j.lithos.2019.02.009>

Reference: LITHOS 4977

To appear in: *LITHOS*

Received date: 17 October 2018

Accepted date: 12 February 2019

Please cite this article as: R.K. Srivastava, V. Guarino, F.-Y. Wu, et al., Evidence of sub-continental lithospheric mantle sources and open-system crystallization processes from in-situ U-Pb ages and Nd–Sr–Hf isotope geochemistry of the cretaceous ultramafic-alkaline-(carbonatite) intrusions from the Shillong Plateau, North-Eastern India, *LITHOS*, <https://doi.org/10.1016/j.lithos.2019.02.009>

This is a PDF file of an unedited manuscript that has been accepted for publication. As a service to our customers we are providing this early version of the manuscript. The manuscript will undergo copyediting, typesetting, and review of the resulting proof before it is published in its final form. Please note that during the production process errors may be discovered which could affect the content, and all legal disclaimers that apply to the journal pertain.

Evidence of sub-continental lithospheric mantle sources and open-system crystallization processes from *in-situ* U–Pb ages and Nd–Sr–Hf isotope geochemistry of the Cretaceous ultramafic-alkaline-(carbonatite) intrusions from the Shillong Plateau, north-eastern India

Rajesh K. Srivastava^a, Vincenza Guarino^{b,*} vincenza.guarino@unina.it, Fu-Yuan Wu^c, Leone Melluso^b, Anup K. Sinha^d

^aDepartment of Geology, Centre of Advanced Study, Banaras Hindu University, Varanasi 221005, India

^bDipartimento di Scienze della Terra, dell'Ambiente e delle Risorse, Università di Napoli Federico II, I-80126 Napoli, Italy

^cState Key Laboratory of Lithospheric Evolution, Institute of Geology and Geophysics, Chinese Academy of Sciences, Beijing 100029, China

^dDr. K.S. Krishnan Geomagnetic Research Laboratory, Indian Institute of Geomagnetism, Allahabad 211505, India

*Corresponding author at: Dipartimento di Scienze della Terra, dell'Ambiente e delle Risorse, Università di Napoli Federico II, Complesso Universitario Monte Sant'Angelo, Ed. L, Via Cintia 26, 80126 Naples, Italy.

ABSTRACT

New *in-situ* U–Pb ages and Sr–Nd–Hf isotopic data on mineral phases of the Sung Valley and Jasra ultramafic-alkaline-(carbonatite) intrusions (Shillong Plateau, India) shed new light on the petrogenetic processes of volcanism in north-eastern India during the Cretaceous. Perovskites of Sung Valley dunite, ijolite and uncomphagrite yielded U–Pb ages of 109.1 ± 1.6 , 104.0 ± 1.3 and 101.7 ± 3.6 Ma, respectively. A U–Pb age of 106.8 ± 1.5 Ma was obtained on zircons of a Sung Valley nepheline syenite. Perovskite of a Jasra clinopyroxenite yielded an age of 101.6 ± 1.2 Ma, different from the U–Pb age of 106.8 ± 0.8 Ma on zircon of Jasra syenites. The variation in Sr–Nd–Hf isotopic compositions [initial $^{87}\text{Sr}/^{86}\text{Sr} = 0.70472$ to 0.71080 ; $\varepsilon_{\text{Nd}\ i} = -10.85$ to $+0.86$; $\varepsilon_{\text{Hf}\ i} = -7.43$ to $+1.52$] matches the bulk-rock isotopic composition of the different rock units of Sung Valley and Jasra. Calcite and apatite in the carbonatites, the perovskite in a dunite, and the bulk-rock carbonatites of Sung Valley intrusion have the lowest initial $^{87}\text{Sr}/^{86}\text{Sr}$ and ε_{Nd} , taken to be the best proxies of the mantle source composition, which is dominated by components derived from the lithospheric mantle. The alkaline intrusions of north-eastern India are significantly younger than the Sylhet tholeiitic magmatism. The silicate rocks of both intrusions have isotopic composition trending to that of the underlying Shillong crust, indicating the effects of fractional crystallization and low-pressure crustal contamination during the emplacement of the various intrusive magma pulses.

Keywords: ultramafic-alkaline-(carbonatite) intrusions; *in-situ* U–Pb ages; Sr–Nd–Hf isotopes; petrogenesis; Shillong Plateau; north-eastern India.

Introduction

The genesis of alkaline igneous intrusions regionally associated with continental flood basalt provinces is always an important aspect to better understand the location of mantle sources in the space, as well as their geochemical and isotopic relationships with the dominant tholeiitic magmatism in the Large Igneous Provinces (LIP) related to the Gondwana dispersal (Bryan and Ernst, 2008; Ernst, 2014; Natali et al., 2018). This mostly because alkaline volcanic rocks are less prone to the effects of crustal contamination during the ascent through the crust than generally evolved, hotter, and more incompatible element-poor, tholeiitic basalts.

Nevertheless, magmas which ponded in crustal reservoirs for significant periods of time are always subject to interaction with continental crust (e.g., De Paolo, 1981), and this effect, better seen through isotopic changes of variably evolved volcanic rocks, must be also recorded in the complementary cumulates and slowly cooled intrusive rocks.

Carbonatitic magmas emplaced in the crust to form igneous rocks are supposed to be derived through different processes: (1) fractional crystallization of primary carbonate-rich nephelinitic magma; (2) immiscible products of variably carbonated nephelinitic-to-phonolitic melts; (3) independent carbonate-rich mantle melts originated by low-degree melting of a carbonated mantle. In the first two cases, a co-genetic relationship can be established between carbonatite and associated silicate rocks; the last one often indicates no petrogenetic relationships between carbonatites and associated silicate rocks (Bell et al., 1998; Mitchell, 2005; Srivastava et al., 2005; Srivastava, 2013; Melluso et al., 2010; Guarino et al., 2017; Beccaluva et al., 2017). Detailed studies on carbonatite and associated silicate magmatic rocks may provide important clues to understand the role of different mantle domains in their genesis (Bell et al., 1998; Srivastava et al., 2005; Guarino et al., 2013, 2017). Carbonatites are some of the very few igneous lithotypes which unambiguously indicate the

presence of CO₂-rich mantle, stable in the form of carbonate-rich lithologies that melted to form magmas (e.g., Song et al., 2017). They show a tendency to preservation of source signatures and related metasomatic processes.

Several Cretaceous ultramafic-alkaline-(carbonatite) [hereafter UA(C)] magmatic intrusions are known in north-eastern India. These intrusions are emplaced within the Shillong Plateau and Mikir Hills (Fig. 1). The Shillong Plateau intrusions comprise Sung Valley (Srivastava and Sinha, 2004a; Srivastava et al., 2005; Melluso et al., 2010), Jasra (Srivastava and Sinha, 2004b, 2007; Melluso et al., 2012), Swangkre-Rongjeng (Srivastava et al., 2016 and references therein), and Mawpyut (Maitra et al., 2011) (Fig. 2a), whereas the Mikir Hills comprise the intrusions of Samchampi and Barpung (Kumar et al., 1996; Saha et al., 2010). These Cretaceous intrusions, together with other Cretaceous magmatism in north-eastern India [e.g., the Rajmahal and Sylhet tholeiitic basalts, the ultrapotassic rocks (lamproites) of the Damodar Valley, such as Jharia, and related mafic dykes] and in the conjugate Antarctic margin (e.g., Beaver Lake ultramafic lamprophyres; Foley et al., 2002) are thought to be igneous products of a mantle plume currently located beneath the Kerguelen archipelago (Storey et al., 1992; Kent et al., 1997, 1998, 2002; Ray et al., 1999; Frey et al., 2002; Srivastava et al., 2009, 2014; Ghatak and Basu, 2011, 2013; Chalapathi Rao et al., 2014). Specifically, the tholeiitic rocks of the Rajmahal-Sylhet tholeiitic basalts are thought to be the direct products of the Kerguelen plume, with components of the Indian Ocean E-MORB and contaminants derived from lower crustal granulites (Ghatak and Basu, 2011, 2013).

The age, petrogenesis, and radiogenic isotope geochemistry for the Sung Valley and the Jasra UA(C) intrusions were already the subject of previous work (Ray et al., 2000; Heaman et al., 2002; Srivastava et al., 2005; Srivastava and Sinha, 2007; Ghatak and Basu, 2013). The petrogenesis of these UA(C) intrusions is still a debated argument; whether different rock units of these intrusions are co-genetic or have been crystallized from independent mantle

melts. Many authors infer that different rock units have a common petrogenetic history, and that late-stage liquid immiscibility played an important role (e.g., Sen, 1999; Ray et al., 2000). However, later studies do not clearly indicate the petrogenesis of the carbonatites through liquid immiscibility processes, rather suggesting that the different rock units were formed by batches of independent magmas with distinct magmatic affinity (Srivastava and Sinha, 2004a, 2004b, 2007; Srivastava et al., 2005; Melluso et al., 2010, 2012). Recent studies proposed that the main rock types (pyroxenites, lamproites, nephelinites, calciocarbonatites and melteigites as Group 1; syenites as Group 2) from Sung Valley, Samchampi, and Barpung, were derived from a primitive carbonated garnet peridotite source in the Kerguelen plume (Group 1), or from low-degree melts of a recycled carbonated eclogite (Group 2) (Ghatak and Basu, 2013). The different isotopic compositions of these two groups are thought to be inherited features of the mantle source (Ghatak and Basu, 2013). We report here new *in-situ* U–Pb ages on zircon and perovskite, and Sr–Nd–Hf isotope data on zircon, perovskite, baddeleyite, apatite, titanite and calcite in Sung Valley and Jasra UA(C) intrusions. The new data would help to discriminate variable crystallization ages of different magmas feeding these intrusions. Additionally, the new *in-situ* Sr–Nd–Hf isotope data on different minerals, linked to those of host rocks, will help to improve understanding the genesis of the magmas feeding these UA(C) intrusions.

Geological setting

The Shillong Plateau is an uplifted horst-like feature, bounded by the Dauki, Brahmaputra, Jamuna and Kopili fault systems (Fig. 2a). The N-S trending Nongchram fault and Um Ngot lineaments and NE-SW trending Badapani-Tyrsad shear zone are other major structural features occurred within the Shillong Plateau. They are thought to be formed during the Late

Jurassic-Early Cretaceous, spatially and temporally associated to the Early Cretaceous ultramafic-mafic-alkaline igneous events (Kumar et al., 1996 and references therein). The Shillong Plateau is formed by Archaean gneisses and Proterozoic mafic dykes (the Shillong Group) and granitic plutons (Fig. 2a; Kumar et al., 1996 and references therein).

The Sung Valley and Jasra intrusions

The petrology and geochemistry of the Sung Valley and Jasra intrusions have been fully presented elsewhere (Srivastava and Sinha, 2004a, 2004b, 2007; Srivastava et al., 2005; Melluso et al., 2010, 2012 and references therein). Detailed petrographic features of Sung Valley and Jasra rocks are reported in the *Supplementary File*.

The Sung Valley intrusion comprises ultramafic silicate rocks (serpentinized perovskite-bearing dunites, wehrlites, and clinopyroxenites, having up to Fo₈₇ olivine and Mg-rich diopsides), uncomphagrites (melilite-rich intrusive rocks), highly alkaline intrusive rocks (ijolites, nepheline syenites) and calciocarbonatites, these latter having up to Fo₉₆ olivine, diopside and phlogopite (Fig. 2b; Srivastava and Sinha, 2004a; Srivastava et al., 2005; Melluso et al., 2010). The peridotites crop out in the central part of the intrusion, and are surrounded by clinopyroxenites. The ijolite body forms a ring structure and intrudes the peridotite. Field setting of different units of the Sung Valley suggests that the ijolite has a discordant relationship with clinopyroxenite, whereas the melilitolite dyke intrudes cumulitic peridotite and clinopyroxenite. Similarly, dykes/veins of nepheline syenite and carbonatite intrude clinopyroxenite and ijolite. These field observations argue against obvious genetic relationships among different rock units (Srivastava and Sinha, 2004a; Srivastava et al., 2005).

The Jasra intrusion comprises olivine-rich ultramafic rocks (olivine up to Fo₈₉, with chromite inclusions, and Mg-rich diopside), clinopyroxenites (some with perovskite), gabbroic rocks (these latter sometimes of subalkaline nature, having Fe-rich olivines with orthopyroxene reaction rims; Melluso et al., 2012), and intrusive syenite/nepheline syenite bodies (mostly dykes) which have also been encountered at a number of places (see Fig. 2c; Srivastava and Sinha, 2004b). A few mafic dykes intrude the clinopyroxenites and the Neoproterozoic host rocks; no mafic dykes are reported to cut the gabbroic intrusions. Srivastava and Sinha (2004a) suggested that these mafic dykes are contemporaneous with the gabbroic intrusions and, therefore, younger than the clinopyroxenites. Small pockets (visible only by hand lenses) of ijolitic and carbonatitic rocks were also observed. Different types of mafic, Mg-rich magmas are thought to have filled the magma chambers that formed the two intrusions, varying from olivine nephelinites/olivine melilitites, perovskite-and/or melilite-bearing, to basanites and alkali basalts. These magmas evolved towards olivine-free nephelinites (forming ijolites), trachytes (forming syenites and melasyenites) and phonolites (forming nepheline syenites) (Melluso et al., 2010, 2012).

Analytical results

Apatite, perovskite, baddeleyite, zircon, titanite, and calcite crystals from sixteen samples from the Sung Valley and Jasra intrusions have been analyzed to obtain *in-situ* U-Pb analyses by SIMS and *in-situ* Sr-Nd-Hf isotope analyses by Laser Ablation (Table 1). The analytical details are reported in the *Appendix: Analytical methods*.

Mineral U-Pb geochronology

Different minerals from six samples, four from Sung Valley and two from Jasra, were analyzed for *in-situ* U-Pb ages. The data are reported in Table 2, Fig. 3 and 4. Table 2 also

reports accurately dated samples from previous studies. Perovskite from SV10, SV31, SV33, JS15P (Fig. 3) and zircon from SV52A and JS5S (Fig. 4) were selected for *in-situ* U-Pb analyses. Perovskite ages of Sung Valley samples vary from 101.7 ± 3.6 Ma from SV33 uncomphahgrite to 109.1 ± 1.6 Ma from SV31 dunite, with 104.0 ± 1.3 Ma from SV10 ijolite. Perovskite age of Jasra clinopyroxenite (sample JS15P) yields 101.6 ± 1.2 Ma, very close to the age of Sung Valley uncomphahgrite. The perovskite separated from a Sung Valley ijolite (sample SV58) yields higher U-Pb TIMS crystallization age of 115.1 ± 5.1 Ma (Srivastava et al., 2005). Most zircons from SV52A nepheline syenite contain very low U concentration, hence low ^{207}Pb ; nevertheless, the $^{206}\text{Pb}/^{238}\text{U}$ age (106.8 ± 1.5 Ma) is thought to be reliable. A consistent U-Pb zircon age of 106.8 ± 0.8 Ma is obtained for a JS5S syenite of the Jasra intrusion. Zircon grains extracted from the same syenite yield U-Pb TIMS age of 105.2 ± 0.5 Ma (Heaman et al., 2002), an age very close to the *in-situ* zircon age obtained in this study.

Sr–Nd–Hf isotopic composition

In-situ Rb-Sr, Sm-Nd and Lu-Hf isotopic data have been through laser ablation techniques. The initial Sr and Nd ratios have been calculated utilizing the ages obtained in this study; in the absence, an average age of 105 Ma has been used (Tables 3, 4, and 5). A significant variation is noted in the $^{87}\text{Sr}/^{86}\text{Sr}$ of mineral separates of various rocks of the Sung Valley intrusion (see Table 3). The initial $^{87}\text{Sr}/^{86}\text{Sr}$ in apatite varies from 0.70474 (carbonatite) to 0.71080 (clinopyroxenite), whereas $^{87}\text{Sr}/^{86}\text{Sr}$ of perovskite varies from 0.70479 (in the dunite) to 0.70956 (in the ijolite). Initial $^{87}\text{Sr}/^{86}\text{Sr}$ of calcite in carbonatite is 0.70472, identical to value obtained for apatite in the same sample. Bulk-rock $^{87}\text{Sr}/^{86}\text{Sr}$ of Sung Valley carbonatites (0.70442-0.70487) are lower than those of associated alkaline silicate rocks (0.70561-0.71078; Table 3). The initial $^{87}\text{Sr}/^{86}\text{Sr}$ in apatite of the silicate samples in the Jasra intrusion ranges from 0.70678 (clinopyroxenite) to 0.70908 (olivine monzodiorite).

Perovskite of clinopyroxenite has the same initial $^{87}\text{Sr}/^{86}\text{Sr}$ (0.70684). The initial $^{87}\text{Sr}/^{86}\text{Sr}$ (0.70652-0.70889; Table 3; Srivastava and Sinha, 2007) of the Jasra rocks matches the isotopic composition of their mineral separates (Table 3).

In-situ Nd isotope data of the Sung Valley intrusion also show significant variations (Table 4). The initial ε_{Nd} values in apatite and baddeleyite of carbonatites and perovskite in dunite (sample SV31) are higher [$\varepsilon_{\text{Nd}\ i} = 0.3\text{-}0.9$ and $\varepsilon_{\text{Nd}\ i} = 0.7$, respectively] than the phases analyzed in the silicate samples [$\varepsilon_{\text{Nd}\ i}$ ranges between -10.8 and 0.7]. Perovskite from the SV33 uncomphagrite has a similar initial ε_{Nd} (+0.6) of the perovskite in the SV31 dunite, whereas perovskite in ijolite has a different initial ε_{Nd} (-2.8). Again, bulk-rock initial ε_{Nd} of carbonatites and silicate samples of the Sung Valley intrusion are close to the values of their mineral phases (Table 4). The initial ε_{Nd} of carbonatites and uncomphagrite [$\varepsilon_{\text{Nd}\ i} = +0.8$ to +1.8 for carbonatites; $\varepsilon_{\text{Nd}\ i} = +0.8$ for S-28 uncomphagrite] is lower than initial ε_{Nd} in the other silicate rocks [$\varepsilon_{\text{Nd}\ i} = -13.10$ to -0.73]. Their neodymium model ages vary between 0.43 and 1.63 Ga. Apatite, titanite and perovskite of the different silicate rocks of Jasra have an initial ε_{Nd} ranging between -4.1 and -0.9 (Table 4), similar to the values of Jasra silicate bulk-rocks [$\varepsilon_{\text{Nd}\ i}$ ranges between -4.8 and -0.7; Table 4], with neodymium model ages of 0.58 – 0.90 Ga.

The Hf isotopic composition of zircon and baddeleyite crystals of Sung Valley and Jasra are reported in Table 5. Zircon of a nepheline syenite (SV52A) has initial $^{176}\text{Hf}/^{177}\text{Hf}$ of 0.282562 and ε_{Hf} of -7.4, while baddeleyite of a carbonatite (SV73) has initial $^{176}\text{Hf}/^{177}\text{Hf}$ of 0.282815 and ε_{Hf} of +1.5. These samples have also variable hafnium model ages ($T_{\text{DM Hf}}$), from 0.96 Ga for nepheline syenite to 0.61 Ga for carbonatite. Baddeleyite and zircon analyzed in the silicate samples of Jasra intrusion have a narrow range of initial $^{176}\text{Hf}/^{177}\text{Hf}$ (0.282668-0.282702) and ε_{Hf} (-3.7 to -2.5) with hafnium model ages ($T_{\text{DM Hf}}$) between 0.76 and 0.82 Ga.

Discussion

The field-setting, bulk-rock geochemical, mineral chemistry, and Sr-Nd isotopic composition of the Sung Valley alkaline carbonatite intrusion do not suggest obvious genetic relationships between constituent rock units (Srivastava and Sinha, 2004a; Srivastava et al., 2005; Melluso et al., 2010). The Jasra rocks derive from perovskite-bearing to orthopyroxene-bearing magmas (Melluso et al., 2012). The rocks of the Jasra intrusion have a slight potassic affinity, whereas those of Sung Valley have sodic affinity (Melluso et al., 2010, 2012).

The ages of Sung Valley and Jasra, and their relationships with the East Indian magmatism of Cretaceous age

The new U-Pb ages of the Sung Valley intrusion, obtained on perovskite from uncomphagrite (SV33), ijolite (SV10), and dunite (SV31) of 101.7 ± 3.6 Ma, 104.0 ± 1.3 Ma and 109.1 ± 1.6 Ma, respectively, indicate quite a prolonged intrusion time. The crystallization age of 106.8 ± 1.5 Ma obtained on zircon in a nepheline syenite (SV52A) is consistent with our new data. These data improve the current data set with new and also different ages than those reported by Ray et al. (1999) on bulk-rock clinopyroxenite (107.2 ± 0.8 Ma, with $^{40}\text{Ar}/^{39}\text{Ar}$ method) and by Ray et al. (2000) on bulk-rock carbonatite and pyroxenite, and phlogopite in carbonatite (106 ± 11 Ma, with Rb-Sr method). The perovskite in the two ijolites yielded different crystallization ages, 104 ± 1.3 Ma (U-Pb SIMS) for sample SV10 and 115 ± 5.1 Ma (U-Pb TIMS; Srivastava et al., 2005) for sample SV58. The age of 115 ± 5.1 Ma (Srivastava et al., 2005) is the oldest obtained for the Sung Valley intrusion, even though is associated with a large analytical uncertainty. The presence of intrusions with distinct crystallization ages at

Sung Valley hampers to establish a definite emplacement sequence. The most plausible hypothesis is that the different intrusive units were produced by independent magma pulses. The age of 106.8 ± 0.8 Ma obtained by a zircon from the JS5S syenite of Jasra is consistent with the age of 105.2 ± 0.5 Ma reported by Heaman et al. (2002), obtained on zircon and baddeleyite from the same syenite. The age of 101.6 ± 1.2 Ma obtained on perovskite in the clinopyroxenite (JS15P) represents the youngest crystallization age reported for Jasra intrusion. The different ages obtained for Jasra syenites and clinopyroxenite again suggest distinct magma batches emplaced at different times.

The U-Pb ages of the Sung Valley and Jasra intrusions (average emplacement age of 105 Ma) are definitely younger than the tholeiitic flood basalts erupted in ~115-118 Ma Rajmahal-Sylhet volcanic province (e.g., Baksi, 1995; Kent et al., 2002). Such a large time span (up to 13 Ma) cannot link the petrogenesis of tholeiitic and alkaline rocks of north-eastern India to a single process, such as melting of a heterogeneous mantle plume, for two main reasons: 1) timing is not that expected, given that the more fusible materials typical of the sources of alkaline magmas should melt at lower temperatures and before, or close to, the main tholeiitic event; 2) a mantle plume having a chemical composition able to contemporaneously generate lamproites, carbonatites + ultra-alkaline and slightly alkaline magmas is “ad hoc” from the fluidodynamic point of view and totally contradictory from the petrological/geochemical points of view. The formation of such strongly different alkaline rocks should imply the stabilization in a hotter-than-normal mantle of low-temperature phases such as amphibole, phlogopite and carbonates, and a substantially anhydrous source typical of flood tholeiites.

Worth to remark that the geochemical characteristics of the Cretaceous lamproites have remarkably common features with the Precambrian lamproites and kimberlites in the eastern India (cf. Chalapathi Rao et al., 2014 and references therein). Current hypotheses about the genesis of alkaline rocks in continental settings prefer their formation after melting

metasomatized lithosphere, able to maintain geochemical heterogeneities and sufficiently thick and cold to make hydrous phases and carbonates stable on the mantle solidus (e.g., Guarino et al., 2013; Melluso et al., 2016; Foley and Fischer, 2017).

The primitive mantle normalized diagrams (Supplementary Figure 1) well highlight distinct patterns and absolute abundances between the various intrusions and rock groups, and provide compelling evidence of chemically distinct sources which undergone different enrichment processes (and variable effects of fractional crystallization).

Sr-Nd-Hf isotope geochemistry of Sung Valley and Jasra rocks and mantle source implications

The close match between the initial $^{87}\text{Sr}/^{86}\text{Sr}$ and ε_{Nd} of the Sung Valley carbonatites and their host phases (apatite, calcite and baddeleyite; Fig. 5, Tables 3 and 4) testify crystallization conditions in a closed magmatic system, and may be taken as the best proxies of the isotopic composition of the mantle source. This source is markedly different from the present-day Indian MORB (Fig. 5). These carbonatites may have crystallized from a melt originated through melting of a metasomatized carbonated mantle (Fig. 7). This carbonate-bearing mantle may also produce melts of olivine melilititic to olivine nephelinitic compositions, which responsible for the crystallization of different silicate rocks after their emplacement in the crust (Srivastava et al., 2005). Indeed, the identical Sr-Nd isotopic composition between the carbonatites and perovskite of the SV31 dunite (Table 1; Fig. 5) indicate that the silicate magma from which the dunite formed could be cogenetic with the carbonatites.

The change of the Sr-Nd isotopes in the alkaline silicate rocks of Sung Valley and Jasra, and the range of U-Pb ages, indicate an open magmatic system (Fig. 5). The SV14 ijolite, S-24

uncompahgrite, and S-69 clinopyroxenite of Sung Valley intrusion have a Sr-Nd isotopic composition intermediate between Sung Valley carbonatites and Jharia lamproites. The Sung Valley syenites and nepheline syenites have the highest initial $^{87}\text{Sr}/^{86}\text{Sr}$ and low initial ε_{Nd} , markedly different from those of more Mg-rich rocks (Fig. 5). The trend towards the underlying Shillong crust indicates contamination during their ponding and emplacement in the Shillong Plateau or, far less likely, of input of crustally derived components in the mantle, which should be most evident in the most felsic lithologies. A similar trend of crustal contamination is observed for the Rajmahal Group II (Kent et al., 1997) and for some Sylhet basalts (Veena et al., 1998; Srivastava et al., 2005; Srivastava and Sinha, 2007; Ghatak and Basu, 2013).

The isotopic composition of Sung Valley and Jasra does not overlap with Indian MORB in the initial ε_{Hf} vs. ε_{Nd} diagram (Fig. 6). The Sung Valley carbonatites and nepheline syenites also have distinct isotopic composition, testifying a change in the isotopic composition of the magmatic system during the formation and emplacement of these rock types.

The Nd and Hf model ages vary from 0.43 to 1.63 Ga for Sung Valley and 0.58 to 0.90 Ga for Jasra (Tables 4 and 5). The range of model ages is similar to that of the Sylhet tholeiitic basalts (0.95-2.36 Ga) and generally similar to that reported for kimberlites and lamproites of the eastern Dharwar craton (1.1-1.4 Ga; Chalapathi Rao et al., 2013), which is generally consistent with the timing of source-enrichment of kimberlites (“orangeites”) in the Bastar craton, Central India (~1.1 Ga; Chalapathi Rao et al., 2011). These data indicate the presence of a regional ultrapotassic-to-sodic, likely pre-Mesozoic, metasomatic event in the lithospheric mantle from the Bengal Basin to the East Antarctica (Fig. 1 and 7). Such heterogeneously enriched mantle generated a large span of low-melt fractions, volatile-rich alkaline magmas, possibly at different depths, and is extremely unlikely to be located in an uprising sub-lithospheric plume, unless contrary evidence. The eruption of the Sylhet-

Rajmahal tholeiitic basalts at ~115-118 Ma, with a source likely located in the spinel-bearing mantle and possibly related to a mantle plume (according to Ghatak and Basu, 2013), was followed at 109-102 Ma by uplift of the Shillong Plateau. In this period, the eruption/intrusion of small degree melts ranging from ultrapotassic to sodic/carbonatitic took place in a peripheral mantle with colder geothermal gradients. These melts derived from the lowermost parts of the Indian/Gondwana lithosphere, enriched by earlier events of metasomatism and that did not suffered interaction with plume-related source compositions (maybe those of the most Mg-rich tholeiitic lavas of Sylhet and Rajmahal). A model for the petrogenesis of the Shillong Plateau alkaline intrusions is reported in the Figure 7.

Conclusions

The new *in-situ* U-Pb ages and Sr-Nd-Hf isotopes highlight different processes involved in the petrogenetic evolution of Sung Valley and the Jasra ultramafic-alkaline-(carbonatite) intrusions:

- 1) The ages for the Sung Valley and Jasra intrusions, estimated to be 102-109 Ma and 102-107 Ma, respectively, suggest emplacement well after the tholeiitic event which generated the Sylhet tholeiitic basalts (117 Ma). This temporal gap (up to 13 Ma) indicates that there is no common relationship with the generation of tholeiitic and alkaline magmatism.
- 2) The Sr-Nd-Hf isotopic composition of the rocks of Sung Valley and Jasra changes with increasing degree of magmatic evolution, indicating the effects of low-pressure crustal contamination, crystal accumulation and fractional crystallization, rather than mantle-derived heterogeneity. This is markedly different from that already supposed for the same rocks and for the Sylhet tholeiitic basalts, and indicate shallow petrogenetic processes following the emplacement in the crust. Of course, no

petrogenetic relationships between the Shillong Plateau alkaline intrusions and the Sylhet anhydrous and substantially incompatible element-depleted tholeiitic magmatism can be hypothesized.

- 3) The isotopic composition of the Sung Valley carbonatites suggests a mantle source different from MORB-asthenosphere, and ultimately located in the lowermost lithospheric mantle of north-eastern India. Carbonatites, Na-ultramafic-alkaline rocks, K-alkaline rocks, the ultrapotassic volcanism of the Damodar Valley, and the Antarctic ultramafic lamprophyres, are all the ultimate result of variable extent and type of metasomatism in the lithospheric mantle of the eastern Gondwana, which probably took place in pre-Mesozoic times.

Acknowledgements

Rajesh K. Srivastava thanks the Head, Department of Geology, Banaras Hindu University, for extending all necessary facilities developed with DST-PURSE grant (Scheme 5050) UGC-CAS-II grant (Scheme 5055). L.M. thanks Fondi Ricerca Dipartimentale during this work. The constructive comments of two anonymous reviewers and advice of the Editor Xian-Hua Li were very useful for the preparation of a revised manuscript.

References

- Baksi, A.K., 1995. Petrogenesis and timing of volcanism in the Rajmahal flood basalt province, northeastern India. *Chemical Geology* 121, 73–90.
- Beccaluva, L., Bianchini, G., Natali, C., Siena, F., 2017. The alkaline-carbonatite complex of Jacupiranga (Brazil): Magma genesis and mode of emplacement. *Gondwana Research* 44, 157–177.

- Bell, K., Kjarsgaard, B.A., Simonetti, A., 1998. Carbonatite-into the twenty-first century. *Journal of Petrology* 39, 1839–1845.
- Bizimis, M., Salters, V.J.M., Dawson, J.B., 2003. The brevity of carbonatite sources in the mantle: evidence from Hf isotopes. *Contribution to Mineralogy and Petrology* 145, 281–300.
- Bryan, S., Ernst, R.E., 2008. Revised definition of Large Igneous Provinces (LIPs). *Earth-Science Reviews* 86, 175–202.
- Chalapathi Rao, N.V., Lehmann, B., 2011. Kimberlites, flood basalts and mantle plumes: New insights from the Deccan Large Igneous Province. *Earth-Science Reviews* 107, 315–324.
- Chalapathi Rao, N.V., Wu, F.-Y., Mitchell, R.H., Li, L.Q., Lehmann, B., 2013. Mesoproterozoic U–Pb ages, trace element and Sr–Nd isotopic composition of perovskite from kimberlites of the Eastern Dharwar craton, southern India: distinct mantle sources and a widespread 1.1 Ga tectonomagmatic event. *Chemical Geology* 353, 48–64.
- Chalapathi Rao, N.V., Srivastava, R.K., Sinha, A.K., Ravikant, V., 2014. Petrogenesis of Kerguelen mantle plume-linked Early Cretaceous ultrapotassic intrusive rocks from the Gondwana sedimentary basins, Damodar Valley, Eastern India. *Earth-Science Reviews* 136, 96–120.
- Chartier, F., Aubert, M., Salmon, M., Tabarant, M., Tran, B.H., 1999. Determination of erbium in nuclear fuels by isotope dilution thermal ionization mass spectrometry and glow discharge mass spectrometry. *Journal of Analytical Atomic Spectrometry* 14, 1461–1465.
- Chaudhuri, S., Ray, J., Koeberl, C., Thöni, M., Dutta, R., Saha, A., Banerjee, M., 2014. Petrology and geochemistry of the ultramafic–mafic Mawpyut complex, Meghalaya: a Sylhet trap differentiation centre in northeastern India. *Geological Journal* 49, 111–128.
- Chauvel, C., Blichert-Toft, J., 2001. A hafnium isotope and trace element perspective on melting of the depleted mantle. *Earth and Planetary Science Letters* 190, 137–151.

- De Paolo, D.J., 1981. Trace element and isotopic effects of combined wallrock assimilation and fractional crystallization. *Earth and Planetary Science Letters* 53, 189–202.
- Doucet, S., Scoates, J.S., Weis, D., Giret, A., 2005. Constraining the components of the Kerguelen mantle plume: a Hf-Pb-Sr-Nd isotopic study of picrites and high-MgO basalts from the Kerguelen archipelago. *Geochemistry Geophysics Geosystems* 6, Q04007.
- Dubois, J.C., Retali, G., Cesario, J., 1992. Isotopic analysis of rare earth elements by total vaporization of samples in thermal ionization mass spectrometry. *International Journal of Mass Spectrometry and Ion Processes* 120, 163–177.
- Ehrlich, S., Gavrieli, I., Dor, L.B., Halicz, L., 2001. Direct high-precision measurements of the $^{87}\text{Sr}/^{86}\text{Sr}$ isotope ratio in natural water, carbonates and related materials by multiple collector inductively coupled plasma mass spectrometry (MC-ICP-MS). *Journal of Analytical Atomic Spectrometry* 16, 1389–1392.
- Ernst, R.E., 2014. Large Igneous Provinces. Cambridge University Press, 653 pp.
- Foley, S.F., Andronikov, A.V., Melzer, S., 2002. Petrology of ultramafic lamprophyres from the Beaver Lake area of Eastern Antarctica and their relation to the breakup of Gondwanaland. *Mineralogy and Petrology* 74, 361–384.
- Foley, S.F., Fischer, T.P., 2017. An essential role for continental rifts and lithosphere in the deep carbon cycle. *Nature Geoscience* 10, 897–902.
- Foster, G.L., Carter, A., 2007. Insights into the patterns and locations of erosion in the Himalaya - A combined fission-track and in situ Sm–Nd isotopic study of detrital apatite. *Earth and Planetary Science Letters* 257, 407–418.
- Frey, F.A., Weis, D., Borisova, A.Yu., Xu, G., 2002. Involvement of continental crust in the formation of the Cretaceous Kerguelen Plateau: new perspectives from the ODP Leg 120 sites. *Journal of Petrology* 43, 1207–1239.

Ghatak, A., Basu, A.R., 2011. The Sylhet Traps: vestiges of the Kerguelen plume in NE India. *Earth and Planetary Science Letters* 308, 52–64.

Ghatak, A., Basu, A.R., 2013. Isotopic and trace element geochemistry of alkalic–mafic–ultramafic–carbonatitic complexes and flood basalts in NE India: origin in a heterogeneous Kerguelen plume. *Geochimica et Cosmochimica Acta* 115, 46–72.

Guarino, V., Wu, F.-Y., Lustrino, M., Melluso, L., Brotzu, P., Gomes, C.B., Ruberti, E., Tassinari, C.C.G., Svisero, D.P., 2013. U-Pb ages, Sr-Nd- isotope geochemistry, and petrogenesis of kimberlites, kamafugites and phlogopite-picrites of the Alto Paranaíba Igneous Province, Brazil. *Chemical Geology* 353, 65–82.

Guarino, V., Wu, F.-Y., Melluso, L., Gomes, C.B., Tassinari, C.C.G., Ruberti, E., Brilli, M., 2017. U-Pb ages, geochemistry, C-O-Nd-Sr-Hf isotopes and petrogenesis of the Catalão II carbonatitic complex (Alto Paranaíba Igneous Province, Brazil): implications for regional-scale heterogeneities in the Brazilian carbonatite associations. *International Journal of Earth Sciences* 106, 1963–1989, doi:10.1007/s00531-016-1402-4.

Heaman, L.M., Srivastava, R.K., Sinha, A.K., 2002. A precise U–Pb zircon/baddeleyite age for the Jasra igneous complex, Karbi-Anglong district, Assam, NE India. *Current Science* 82, 744–748.

Ingle, S., Weis, D., Frey, F.A., 2002. Indian continental crust recovered from Elan Bank, Kerguelen Plateau (ODP Leg 183, Site 1137). *Journal of Petrology* 43, 1241–1257.

Ingle, S., Weis, D., Doucet, S., Mattielli, N., 2003. Hf isotope constraints on mantle sources and shallow-level contaminants during Kerguelen hot spot activity since 120 Ma. *Geochemistry Geophysics Geosystems* 4, 1068.

Ireland, T.R., Compston, W., Williams, I.S., Wendt, I., 1990. U-Th-Pb systematics of individual perovskite grains from the Allende and Murchison carbonaceous chondrites. *Earth and Planetary Science Letters* 101, 379–387.

Isnard, H., Brennetot, R., Caussignac, C., Caussignac, N., Chartier, F., 2005. Investigations for determination of Gd and Sm isotopic compositions in spent nuclear fuels samples by MC ICPMS. International Journal of Mass Spectrometry 246, 66–73.

Jackson, M.G., Weis, D., Huang, S., 2012. Major element variations in Hawaiian shield lavas: Source features and perspectives from global ocean island basalt (OIB) systematics. Geochemistry Geophysics Geosystems 13, Q09009, doi:10.1029/2012GC004268.

Kent, R.W., Saunders, A.D., Kempton, P.D., Ghose, N.C., 1997. Rajmahal basalts, eastern India: mantle source and melt distribution at a volcanic rifted margin. In: Mahoney, J.J., Coffin, M.F. (Eds.), Large Igneous Provinces – Continental, Oceanic and Planetary Flood Volcanism, A.G.U. Geophysical Monograph Series 100, pp. 145–182.

Kent, R.W., Kelley, S.P., Pringle, M.S., 1998. Mineralogy and $^{40}\text{Ar}/^{39}\text{Ar}$ geochronology of orangeites (Group II kimberlites) from the Damodar valley, eastern India. Mineralogical Magazine 63, 313–323.

Kent, R.W., Pringle, M.S., Müller, R.D., Saunders, A.D., Ghose, N.C., 2002. $^{40}\text{Ar}/^{39}\text{Ar}$ geochronology of the Rajmahal basalts, India, and their relationship to the Kerguelen Plateau. Journal of Petrology 43, 1141–1153.

Kumar, D., Mamallan, R., Dwivedy, K.K., 1996. Carbonatite magmatism in northeast India. Journal of Asian Earth Sciences 13(2), 145–158.

Kumar, A., Dayal, A.M., Padmakumari, V.M., 2003. Kimberlite from Rajmahal magmatic province: Sr–Nd–Pb isotopic evidence for Kerguelen plume derived magmas. Geophysical Research Letters 30, 2053–2056.

Li, Q.L., Li, X.H., Liu, Y., Tang, G.Q., 2010a. Precise U–Pb and Pb–Pb dating of Phanerozoic baddeleyite by SIMS with oxygen flooding technique. Journal of Analytical Atomic Spectrometry 25, 1107–1113.

- Li, Q.L., Li, X.H., Liu, Y., Wu, F.-Y., Yang, J.H., Mitchell, R.H., 2010b. Precise U–Pb and Th–Pb age determination of kimberlitic perovskites by secondary ion mass spectrometry. *Chemical Geology* 269, 396–405.
- Li, X.H., Liu, Y., Li, Q.L., Guo, C.H., Chamberlain, K.R., 2009. Precise determination of Phanerozoic zircon Pb/Pb age by multi-collector SIMS without external standardization. *Geochemistry Geophysics Geosystems* 10, Q04010, doi: 10.1029/2009GC00 2400.
- Lyubetskaya, T., Korenaga, J., 2007. Chemical composition of Earth's primitive mantle and its variance: 1 Method and results. *Journal of Geophysical Research* B112, 1–21.
- Ludwig, K.R., 2003. User's Manual for Isoplot 3.00: A Geochronological Toolkit for Microsoft Excel. Berkeley Geochronology Center Special Publication, Berkeley 4, 70 pp.
- Mahoney, J.J., Graham, D.W., Christie, D.M., Johnson, K.T.M., Hall, L.S., Vonderhaar, D.L., 2002. Between a hotspot and a cold spot: isotopic variation in the Southeast Indian Ridge asthenosphere, 86°E–118°E. *Journal of Petrology* 43, 1155–1176.
- Maitra, M., David, J.S., Bhaduri, S., 2011. Melanite garnet-bearing nepheline syenite minor intrusion in Mawpyut ultramafic-mafic complex, Jaintia Hills, Meghalaya. *Journal of Earth System Science* 120, 1033–1041.
- Mattielli, N., Weis, D., Blachert-Toft, J., Albaréde, F., 2002. Hf isotope evidence for a Miocene change in the Kerguelen mantle plume composition. *Journal of Petrology* 43, 1327–1339.
- McFarlane, C.R.M., McCulloch, M.T., 2007. Coupling of in-situ Sm–Nd systematics and U–Pb dating of monazite and allanite with applications to crustal evolution studies. *Chemical Geology* 245, 45–60.
- Melluso, L., Cucciniello, C., le Roex, A.P., Morra, V., 2016. The geochemistry of primitive volcanic rocks of the Ankaratra volcanic complex, and source enrichment processes in the

genesis of the Cenozoic magmatism in Madagascar. *Geochimica et Cosmochimica Acta* 185, 435–452. <https://dx.doi.org/10.1016/j.gca.2016.04.005>.

Melluso, L., Srivastava, R.K., Guarino, V., Zanetti, A., Sinha, A.K., 2010. Mineral chemistry and petrogenetic evolution of the ultramafic–alkaline–carbonatitic complex of Sung Valley, Northeastern India. *The Canadian Mineralogist* 48, 205–229.

Melluso, L., Srivastava R.K., Petrone, C.M., Guarino, V., Sinha, A.K., 2012. Mineralogy and magmatic affinity of the Jasra Intrusive Complex, Shillong Plateau, India. *Mineralogical Magazine* 76(5), 1099–1117.

Mitchell, R.H., 2005. Carbonatites and carbonatites and carbonatites. *The Canadian Mineralogist* 43, 2049–2068.

Morel, M.L.A., Nebel, O., Nebel-Jacobsen, Y.J., Miller, J.S., Vroon, P.Z., 2008. Hafnium isotope characterization of the GJ-1 zircon reference material by solution and laser-ablation MC-ICPMS. *Chemical Geology* 255, 231–235.

Natali, C., Beccaluva, L., Bianchini, G., Siena, F., 2018. Coexistence of alkaline–carbonatite complexes and high-MgO CFB in the Paranà-Etendeka province: Insights on plume-lithosphere interactions in the Gondwana realm. *Lithos* 296–299, 54–66.

Ramos, F.C., Wolff, J.A., Tollstrup, D.L., 2004. Measuring $^{87}\text{Sr}/^{86}\text{Sr}$ variation in minerals and groundmass from basalts using LA–MC–ICP–MS. *Chemical Geology* 211, 135–158.

Ray, J.S., Ramesh, R., Pande, K., 1999. Carbon isotopes in Kerguelen plume – derived carbonatites: evidence for recycled inorganic carbon. *Earth and Planetary Science Letters* 170, 205–214.

Ray, J.S., Trivedy, J.R., Dayal, A.M., 2000. Strontium isotope systematics of Amba Dongar and Sung Valley carbonatite-alkaline complexes, India: evidence for liquid immiscibility, crustal contamination and long-lived Rb/Sr enriched mantle sources. *Journal of Asian Earth Sciences* 18, 585–594.

Ray, J., Saha, A., Koeberl, C., Thoni, M., Ganguly, S., Hazra, S., 2013. Geochemistry and petrogenesis of Proterozoic mafic rocks from east Khasi Hills, Shillong Plateau, northeastern India. *Precambrian Research* 230, 119–137.

Saha, A., Ganguly, S., Ray, J., Chatterjee, N., 2010. Evaluation of phase chemistry and petrochemical aspects of Samchampi-Samteran differentiated alkaline complex of Mikir Hills, northeastern India. *Journal of Earth System Science* 119(5), 675–699.

Saha, A., Ganguly, S., Ray, J., Koeberl, C., Thöni, M., Sarabajana, C., Sawant, S.S., 2017. Petrogenetic evolution of Cretaceous Samchampi-Samteran Alkaline Complex, Mikir Hills, Northeastern India: Implications on multiple melting events of heterogeneous plume and metasomatized sub-continental lithospheric mantle. *Gondwana Research* 48, 237–256.

Sen, A.K., 1999. Origin of the Sung Valley carbonatite complex, Meghalaya, India: major element geochemistry constraints. *Journal of the Geological Society of India* 53, 285–297.

Sláma, J., Košler, J., Condon, D.J., Crowley, J.L., Gerdes, A., Hanchar, J.M., Whitehouse, M.J., 2008. Plešovice zircon – a new natural reference material for U–Pb and Hf isotopic microanalysis. *Chemical Geology* 249, 1–35.

Song, W.-L., Xu, S., Chakhmouradian, A.R., Kynicky, J., Huang, K., Zhang, Z-L., 2017. Carbonatites of Tarim (NW China): First evidence of crustal contribution in carbonatites from a large igneous province. *Lithos* 282-283, 1–9.

Srivastava, R.K., 2013. Petrological and geochemical characteristics of Paleoproterozoic ultramafic lamprophyres and carbonatites from the Chitrangi region, Mahakoshal supracrustal belt, central India. *Journal of Earth System Science* 122(3), 759–776.

Srivastava, R.K., Sinha, A.K., 2004a. The early Cretaceous Sung Valley ultramafic–alkaline–carbonatite complex, Shillong Plateau, northeastern India: petrological and genetic significance. *Mineralogy and Petrology* 80, 241–263.

Srivastava, R.K., Sinha, A.K., 2004b. Geochemistry of early Cretaceous alkaline ultramafic-mafic complex from Jasra, Karbi Anglong, Shillong plateau, Northeastern India. *Gondwana Research* 7, 549–561.

Srivastava, R.K., Sinha, A.K., 2007. Nd and Sr isotope systematic and geochemistry of plume related early Cretaceous alkaline-mafic-ultramafic-igneous complex from Jasra, Shillong Plateau, Northeastern India. *Geological Society of America Special Papers* 430, 815–830.

Srivastava, R.K., Chalapathi Rao, N.V.C., Sinha, A.K., 2009. Cretaceous potassic intrusives with affinities to aillikites from Jharia area: Magmatic expression of metasomatically veined and thinned lithospheric beneath Singhbhum Craton, Eastern Indian. *Lithos* 112, 407–418.

Srivastava, R.K., Heaman, L.M., Sinha, A.K., Shihua, S., 2005. Emplacement age and isotope geochemistry of Sung Valley alkaline-carbonatite complex, Shillong Plateau, northeastern India: implications for primary carbonate melt and genesis of the associated silicate rocks. *Lithos* 81, 33–54.

Srivastava, R.K., Kumar, S., Sinha, A.K., Chalapathi Rao, N.V., 2014. Petrology and geochemistry of high-titanium and low-titanium mafic dykes from the Damodar valley, Chhotanagpur Gneissic Terrain, eastern India and their relation to mantle plume(s). *Journal of Asian Earth Sciences* 84, 34–50.

Srivastava, R.K., Melluso, L., Sinha A.K., 2016. Petrogenesis of an early Cretaceous potassic lamprophyre dyke from Rongjeng, East Garo Hills, Shillong plateau, north-eastern India. *Current Science* 110(4), 649–658.

Stacey, J.S., Kramers, J.D., 1975. Approximation of terrestrial lead isotope evolution by a two-stage model. *Earth and Planetary Science Letters* 26, 207–221.

- Storey, M., Kent, R.W., Saunders, A.D., Salters, V.J., Hergt, J.M., Whitechurch, H., Sevigny, J.H., Thirlwall, M.F., Leat, P.T., Ghose, N.C., Gifford, M., 1992. Lower Cretaceous volcanic rocks on continental margins and their relationship to the Kerguelen Plateau. In: S.W. Wise and R. Schlich, et al. (Eds.), Proceeding Ocean Drilling Program Scientific Results 120, College Station, TX, pp. 33–53.
- Tappe, S., Pearson, D.G., Kjarsgaard, B.A., Nowell, G.M., Dowall, D., 2013. Mantle transition zone input to kimberlite magmatism near a subduction zone: origin of anomalous Nd–Hf isotope systematics at Lac de Gras, Canada. *Earth and Planetary Science Letters* 371–372, 235–251.
- Tappe, S., Kjarsgaard, B.A., Kurszlaukis, S., Nowell, G.M., Phillips, D., 2014. Petrology and Nd-Hf isotope geochemistry of the Neoproterozoic Amon Kimberlite Sills, Baffin Island (Canada): evidence for deep mantle magmatic activity linked to supercontinent cycles. *Journal of Petrology* 55, 2003–2042.
- Veena, K., Pandey, B.K., Krishnamurthy, P., Gupta, J.N., 1998. Pb, Sr, and Nd isotope systematics of carbonatites of Sung Valley, Meghalaya, North East India: implications for contemporary plume related mantle source characteristics. *Journal of Petrology* 39, 1875–1884.
- Vervoort, J.D., Patchett, P.J., Soderlund, U., Baker, M., 2004. Isotopic composition of Yb and the determination of Lu concentrations and Lu/Hf ratios by isotopic dilution using MC-ICP-MS. *Geochemistry Geophysics Geosystems* 5, Q11002, doi:10.1029/2004GC000721.
- Wasserburg, G.J., Jacobsen, S.B., DePaolo, D.J., McCulloch, M.T., Wen, T., 1981. Precise determination of Sm/Nd ratios, Sm and Nd isotopic abundances in standard solutions. *Geochimica et Cosmochimica Acta* 45, 2311–2323.

- Wiedenbeck, M., Allé, P., Corfu, F., Griffin, W.L., Meier, M., Oberli, F., Von Quadt, A., Roddick, J.C., Spiegel, W., 1995. Three natural zircon standards for U–Th–Pb, Lu–Hf, trace-element and REE analyses. *Geostandards and Geoanalytical Research* 19, 1–23.
- Wu, F.-Y., Yang, Y.H., Xie, L.W., Yang, J.H., Xu, P., 2006. Hf isotopic compositions of the standard zircons and baddeleyites used in U-Pb geochronology. *Chemical Geology* 234, 105–126.
- Wu, F.-Y., Arzamastsev, A.A., Mitchell, R.H., Li, Q.L., Sun, J., Yang, Y.H., Wang, R.C., 2013. Emplacement age and Sr-Nd isotopic compositions of the Afrikanda alkaline ultramafic complex, Kola Peninsula, Russia. *Chemical Geology* 353, 210–229.
- Xie, L.W., Zhang, Y.B., Zhang, H.H., Sun, J.F., Wu, F.-Y., 2008. *In situ* simultaneous determination of trace elements, U–Pb and Lu–Hf isotopes in zircon and baddeleyite. *Chinese Science Bulletin* 53, 1565–1573.
- Yang, Y.H., Sun, J.F., Xie, L.W., Fan, H.R., Wu, F.-Y., 2008. *In-situ* Nd isotopic measurements of geological samples by laser ablation. *Chinese Science Bulletin* 53, 1062–1070.
- Yang, Y.H., Wu, F.-Y., Yang, J.H., Chew, D.M., Xie, L.W., Chu, Z.Y., Zhang, Y.B., Huang, C., 2014. Sr and Nd isotopic compositions of apatite reference materials used in U-Th-Pb geochronology. *Chemical Geology* 385, 35–55.

Appendix A. Analytical methods

Eight samples of Sung Valley and eight samples of Jasra, based on petrographic features and mineral chemistry (Melluso et al., 2010, 2012), were chosen for *in-situ* Sr-Nd-Hf isotope analyses of apatite, perovskite, zircon, baddeleyite, titanite, and calcite using laser ablation (MC-ICP-MS) (Table 1). Out of these sixteen samples, six (four from the Sung Valley intrusion and two from the Jasra intrusion) were selected for the *in-situ* U-Pb analyses of perovskite, zircon and baddeleyite using SIMS (Table 2).

In-situ U-Pb analyses by SIMS. The *in-situ* U-Pb analyses of perovskite, zircon and baddeleyite grains were performed by using the CAMECA1280 ion microprobe, installed at the Institute of Geology and Geophysics in Beijing. The samples were mounted in epoxy and coated with about 30 μm of high-purity gold to reach $<20 \Omega$ resistance. The instrument description and analytical procedure can be found in Li et al. (2009, 2010a, 2010b) and Wu et al. (2013); a very summary is given here. The O^{2-} primary ion beam was accelerated at -13 kV, with an intensity of $\sim 10 \text{nA}$. Sample charging effects were minimized by optimizing the energy offset to maximum transmission in a 60 eV energy window at the start of each analysis. A single electron multiplier was used in the ion-counting mode to measure secondary ion beam intensities by a peak jumping sequence.

Perovskite U-Pb ages. A total sequence includes the Pb^+ species, Th^+ , U^+ , ThO^+ , UO_2^+ and $^{40}\text{Ca}^{48}\text{Ti}_2^{16}\text{O}_4$ species to produce one set of data. The peak of $^{40}\text{Ca}^{48}\text{Ti}_2^{16}\text{O}_4$ is used as a matrix reference for centering the secondary ion beam, energy and mass adjustments, as well as reference for mass 200.5 (background). A mass resolution of ca. 8000 (defined at 50% peak height) was used to separate U, Th, and Pb isotopes from isobaric interferences. Each measurement consisted of 10 cycles, and the total analytical time was ca. 16 min. A Tazheran perovskite (463 Ma; Ireland et al., 1990) was used as reference materials to calibrate the Pb/U

fractionation. The Ice River perovskite was used as unknown to monitor the whole analytical procedure.

Zircon U-Pb ages. Oxygen flooding was used to increase the O₂ pressure to $\sim 5 \times 10^{-6}$ Torr in the sample chamber, enhancing Pb⁺ sensitivity to a value of 25–28 cps/nA/ppm for zircon (Li et al., 2009, 2010a). A mass resolution of ~ 7000 (at 50% peak height) was used, and the magnet was cyclically peak-stepped through a sequence including the Pb⁺ species, U⁺, ThO⁺, UO₂⁺ and Zr₂O species to produce one set of data. The ⁹⁰Zr₂¹⁶O signal was used as reference peak for centering secondary ion beams. Each measurement consists of 7 cycles, and the total analytical time is ~ 12 min. For zircon U-Pb age determinations, Pb/U ratios were calibrated with a power law relationship between Pb/U and UO₂/U relative to the standard zircon Plesovice, having an age of 337 Ma (Sláma et al., 2008). Calibration of Th and U concentrations and Th/U ratios were based on standard zircon 91500 with concentration of Th and U of ~ 29 and ~ 81 ppm, respectively (Wiedenbeck et al., 1995). A long-term uncertainty of 1.5% (1 RSD) for ²⁰⁶Pb/²³⁸U measurements of the Plesovice standard was propagated to the unknowns, regardless that the measured ²⁰⁶Pb/²³⁸U error in a specific session is generally around 1% (1 RSD) or less (Li et al., 2010a).

The measured Pb isotopic compositions were corrected for common Pb using non-radiogenic ²⁰⁴Pb measured. Small corrections are insensitive to the choice of common Pb composition, and hence an average of present-day crustal composition (Stacey and Kramers, 1975) is used for the common Pb assuming that the common Pb is largely surface contamination introduced during sample preparation. Uncertainties of individual analyses are reported at a 1σ level; and mean ages for pooled U/Pb (and Pb/Pb) analyses quoted with a 95% confidence interval. Data reduction was carried out using the Isoplot/Ex v. 3.0 program (Ludwig, 2003).

In-situ Sr-Nd-Hf isotopic analyses by laser ablation. The *in-situ* Sr–Nd–Hf isotopic analyses were conducted using a Neptune MC-ICP-MS instrument. Detailed analytical protocols are

given by Xie et al. (2008), Yang et al. (2008, 2014) and Wu et al. (2006); however, few important information about these analyses are reported here.

The *in-situ* Sr isotopic data were acquired in static, multi-collector mode with low resolution using nine Faraday collectors, and the mass configuration array from ^{83}Kr to ^{88}Sr , monitoring Kr and Rb, which is identical to the technique of Ramos et al. (2004). Prior to analysis, collectors were aligned using a tuning solution which contains Rb, Sr, Er, and Yb. An aliquot of 200 ppb NBS 987 (NIST SRM 987) was regularly used to check quality and optimizing the operation parameters, including the torch position. During laser ablation analysis, various interferences were evaluated. Prior to every analytical session, the Neptune MC–ICP–MS was always set-up to monitor Kr in the Ar gas after optimization, especially when a new liquid Ar tank was replaced. During analyses, 50s measurement of the gas blank was carried out prior to ablation to correct Kr, like the method employed by Ramos et al. (2004). The natural ratio of $^{85}\text{Rb}/^{87}\text{Rb}=2.5926$ was used for isobaric correction of Rb by an exponential law, assuming that rubidium has the same mass discrimination as strontium (Ehrlich et al., 2001). No correction was applied for the interference of Ca argide/dimmer species since it has been demonstrated that this interference is negligible (e.g., Ehrlich et al., 2001; Ramos et al., 2004; Yang et al., 2014). Interferences from Fe dioxides, and Ga and Zn oxides, were not considered in this study, due to their low signals during analysis. Interference from the doubly-charged rare earth elements (REEs) cannot be considered as negligible for pyrochlore, as this phase has high concentrations of REEs. Based on the method proposed by Ramos et al. (2004), we monitored the presence of $^{167}\text{Er}^{2+}$, $^{171}\text{Yb}^{2+}$ and $^{173}\text{Yb}^{2+}$ at masses 83.5, 85.5 and 86.5. Then the contributions of $^{168}\text{Er}^{2+}$ and $^{168}\text{Yb}^{2+}$ to ^{84}Sr , $^{170}\text{Er}^{2+}$ and $^{170}\text{Yb}^{2+}$ to ^{85}Rb , $^{172}\text{Yb}^{2+}$ to ^{86}Sr , $^{174}\text{Yb}^{2+}$ to ^{87}Sr (+ ^{87}Rb), and $^{176}\text{Yb}^{2+}$ to ^{88}Sr were calculated according to the isotopic abundances of Er and Yb (Chartier et al., 1999; Vervoort et al., 2004). Perovskite from the Afrikanda complex was used as an external standard during the analyses; it give a weighted

$^{87}\text{Sr}/^{86}\text{Sr}$ value of 0.70335 ± 2 (2s, n=33), which agrees well with the recommended value of 0.70335 reported in Wu et al. (2013).

The *in-situ* Nd isotope technique is like that for Sr described above. The spot size used was 40–60 μm with a 4–10 Hz pulse rate according to Nd concentration of ablated minerals. As in all laser ablation methodologies, great care must be taken to avoid or mitigate the effects of isobaric interferences. For *in-situ* Nd isotopic analyses, the interferences are principally caused by Ce (^{142}Ce on ^{142}Nd) and Sm (^{144}Sm on ^{144}Nd). However, our work indicates that the influence of Ce on Nd isotopic analysis is insignificant when the Ce/Nd ratio is 3, which is a reasonable value in natural geological materials (Yang et al., 2009). The most crucial aspect during *in-situ* Nd isotope measurement is how to precisely determine the isobaric interference of ^{144}Sm on ^{144}Nd , especially determination of the mass bias of Sm (β_{Sm}) (Foster and Carter, 2007; McFarlane and McCulloch, 2007). In this study, the β_{Sm} value was obtained directly from the $^{147}\text{Sm}/^{149}\text{Sm}$ ratio on the sample itself and then applied in the isobaric interference correction of ^{144}Sm on ^{144}Nd , following the method proposed by McFarlane and McCulloch (2007). We also used the $^{147}\text{Sm}/^{149}\text{Sm}$ ratio of 1.08680 (Dubois et al., 1992) and $^{144}\text{Sm}/^{149}\text{Sm}$ ratio of 0.22332 (Isnard et al., 2005), as determined by MC–ICP–MS, in data reduction (Yang et al., 2008). Furthermore, the $^{145}\text{Nd}/^{144}\text{Nd}$ ratio was used to evaluate the feasibility of our method since it has a constant value of 0.348415 obtained by TIMS (Wasserburg et al., 1981). During analyses, in-house standard of the AFK perovskite is used. It yielded an average $^{143}\text{Nd}/^{144}\text{Nd} = 0.512602 \pm 6$ (2s, n=32), consistent with the recommended value of 0.512609 (Wu et al., 2013).

The MC-ICPMS, used to obtain Hf isotopic composition, operated in static mode with the integration for baseline of 30 s. The signal collection model is one block with 200 cycles, in which one cycle has 0.131 s integration time. Total time is about 30 s during each analysis. The parameters applied in the study are 15 J/cm² of energy density, 50 μm of spot size and 8

Hz of ablation frequency. Interferences of ^{176}Lu and ^{176}Yb on ^{176}Hf were corrected according to a procedure described in Wu et al. (2006). The analyses were obtained using the same mounts which were previously used for U–Pb dating. During analytical sessions, the $^{176}\text{Hf}^{177}\text{Hf}$ value obtained for 91500 and GJ-1 were 0.282307 ± 9 (2s, n=23) and 0.282029 ± 19 (2s, n=11), respectively, which agree well with the recommended values of 0.282305 and 0.282000 from the literature (Wu et al., 2006; Morel et al., 2008).

Figure captions

Figure 1. Geological sketch map of north-eastern India showing the location of Late Cretaceous magmatic activity in the Damodar Valley, Rajmahal and Sylhet tholeiitic basalts, the Shillong Plateau, and the Mikir Hills (Srivastava et al., 2016). The *inset* shows the area of reference.

Figure 2. a) Regional geological and tectonic setup of the Shillong Plateau (modified from Srivastava and Sinha, 2004a, 2004b). Legend: 1. Cretaceous–Tertiary sediments; 2. Ultramafic-alkaline-(carbonatite) intrusions [dashed circles are: (1) Sung Valley; (2) Jasra; (3) Rongjeng–Swangkre; (4) Mawpyut]; 3. Sylhet tholeiitic basalts; 4. Archean gneissic complex, Shillong Group rocks, mafic igneous rocks, and Proterozoic granites; 5. Major fault systems; 6. Alluvium and recent sediments. b) Geological map of the Sung Valley ultramafic-alkaline-carbonatite intrusion (after Srivastava and Sinha, 2004a; Srivastava et al., 2005). Nepheline syenite and melilitolite dykes exposed around the Sung and Maskut villages are very small, hence not mentioned on the map. Location of samples, analyzed here, is also shown. c) Geological map of the Jasra alkaline-ultramafic-mafic intrusion (after Srivastava and Sinha, 2004b, 2007). Legend: 1: Shillong Group rocks; 2: Neoproterozoic granite; 3: pyroxenite; 4: gabbro; 5: mafic dyke exposures; 6: nepheline syenite exposures. Locations of samples, analyzed here, are also shown.

Figure 3. U-Pb age determination results (error in 2σ) for perovskite from the Sung Valley (SV) and the Jasra (JS) ultramafic-alkaline-(carbonatite) intrusions, NE India.

Figure 4. U-Pb age determination results (error in 2σ) for zircon from the Sung Valley (SV) and the Jasra (JS) ultramafic-alkaline-(carbonatite) intrusions, NE India.

Figure 5. The initial ε_{Nd} and $^{87}\text{Sr}/^{86}\text{Sr}$ diagram for the new isotopic data from the Sung Valley (SV) and the Jasra (JS) ultramafic-alkaline-(carbonatite) intrusions, NE India. The reported bulk-rock analyses are from (1) Srivastava et al. (2005), (2) Veena et al. (1998), (3) Ghatak

and Basu (2013), and (4) Srivastava and Sinha (2007). Isotopic variations in Kerguelen basalts are from Storey et al. (1992), Mahoney et al. (2002 and references therein), Kumar et al. (2003); compiled in Srivastava et al. (2005), Srivastava and Sinha (2007), Ghatak and Basu (2013), and Mattielli et al. (2002), Ingle et al. (2003), Doucet et al. (2005); Rajmahal tholeiitic basalts of Group I and Group II are from Storey et al. (1992), Baksi (1995) and Kent et al. (1997); Sylhet tholeiitic basalts from Ghatak and Basu (2011); Mawpyut complex from Chaudhuri et al. (2014); East Khasi Hills from Ray et al. (2013); Samchampi-Samteran Alkaline Complex from Saha et al. (2017); Jharia lamproites from Kumar et al. (2003). The continental clasts from IODP site 1137 are from Ingle et al. (2002). The Indian MORB is from Mahoney et al. (2002). The data on the Hawaii Islands are from Jackson et al. (2012) and references therein.

Figure 6. The initial ϵ_{Hf} vs. ϵ_{Nd} diagram for the Sung Valley and the Jasra ultramafic-alkaline-(carbonatite) intrusions, NE India. The fields of Indian MORB (Chauvel and Blichert-Toft, 2001), Kerguelen basalts (Mattielli et al., 2002; Ingle et al., 2003; Doucet et al., 2005), Canadian carbonatites and lamprophyres (Bizimis et al., 2003; Tappe et al., 2013, 2014), Catalão I alkaline-carbonatite complex (Guarino et al., 2017) and global OIB and Hawaii Islands (Jackson et al., 2012 and references therein) are shown for comparison.

Figure 7. A schematic model (not to scale) showing age progression of volcanism of NE India and different enrichment processes starting from Shillong (Jasra and Sung Valley) to the East Antarctica and Kolkata areas (Beaver Lake ultramafic lamprophyres, Foley et al., 2002; Jharia lamproites, Kumar et al., 2003). These processes are related to two different stages, at ~118-115 Ma with emplacement of Rajmahal and Sylhet tholeiitic basalts from Kerguelen plume, and at ~109-102 Ma, which correspond to intrusion and open-system crystallization of various intrusions in areas not involved by any plume-related

thermochemical effect. Abbreviations: UAC, ultramafic-alkaline-carbonatite; UA, ultramafic-alkaline.

Table captions

Table 1. List of samples and analyzed minerals for *in situ* U-Pb analyses by SIMS and *in situ* Sr-Nd-Hf isotope analyses by LA-ICP-MS.

Table 2. Geochronological data of Sung Valley and Jasra intrusions, Shillong Plateau, NE India.

Table 3. Sr isotope composition of different minerals/ and bulk-rocks of Sung Valley and Jasra intrusions, Shillong Plateau, NE India.

Table 4. Nd isotope composition of minerals/ and bulk-rocks of Sung Valley and Jasra intrusions, Shillong Plateau, NE India.

Table 5. Hf isotope data of different minerals of Sung Valley and Jasra intrusions, Shillong Plateau, NE India.

Supplementary File:

Supplementary File. Petrography of Sung Valley and Jasra rocks selected for U-Pb and Sr-Nd-Hf analyses.

Supplementary Figure 1. Primitive mantle normalized diagrams for the rock types of Sung Valley and Jasra, together with those of other Indian or Antarctic tholeiitic and alkaline rocks (Sylhet tholeiitic basalts, Sahibganj, Tinpahar, Harinsingha and Taljhari basaltic flows; alkaline rocks of Jharia, Raniganj, Swangkhre, Beaver Lake, Samchampi, Barpung, Bokaro and Sikkim; data from Srivastava et al., 2016 and Ghatak and Basu, 2013 and references therein).

Table 1 List of samples and analyzed minerals for in situ U-Pb analyses by SIMS and in situ Sr-Nd-Hf isotope analyses by LA-ICP-MS

S. No.	Sample No.	Rock type	Analyzed minerals	Type of analyses
Samples from the Sung Valley intrusion				
1	SV 7	Clinopyroxenite	Apatite	Sr and Nd isotopes
2	SV10	Ijolite	Perovskite	Sr and Nd isotopes, <i>U-Pb age</i>
			Apatite	Sr and Nd isotopes
3	SV25	Nepheline syenite	Apatite	Sr and Nd isotopes
4	SV31	Dunite	Perovskite	Sr and Nd isotopes, <i>U-Pb age</i>
5	SV33	Uncompahgrite	Perovskite	Sr and Nd isotopes, <i>U-Pb age</i>
			Apatite	Sr isotope
6	SV52A	Nepheline syenite	Zircon	Hf isotope, <i>U-Pb age</i>
			Apatite	Sr and Nd isotopes
7	SV73	Carbonatite	Baddeleyite	Nd and Hf isotopes
			Apatite	Sr and Nd isotopes
			Calcite	Sr isotope
8	SV83	Ijolite	Apatite	Sr isotope
Samples from the Jasra intrusion				
1	JS2	Essexite	Apatite	Sr and Nd isotopes
2	JS5G	Nepheline monzodiorite	Baddeleyite	Hf isotope
			Apatite	Sr and Nd isotopes
3	JS5S	Syenite	Baddeleyite	Hf isotope
			Zircon	Hf isotope, <i>U-Pb age</i>
			Apatite	Sr and Nd isotopes
4	JS15P	Clinopyroxenite with intruded syenite	Perovskite	Sr and Nd isotopes, <i>U-Pb age</i>
			Titanite	Nd isotope
			Apatite	Sr and Nd isotopes
5	JS16	Clinopyroxenite	Apatite	Sr and Nd isotopes
6	JS34	Olivine monzodiorite	Apatite	Sr and Nd isotopes
7	JS39	Shonkinit	Titanite	Nd isotope
			Apatite	Sr and Nd isotopes
8	JS42	Amphibole monzodiorite	Apatite	Sr and Nd isotopes

Table 2 Geochronological data of Sung Valley and Jasra intrusions, Shillong Plateau, NE India.

	Material/Sample No.	Method	Age (Ma)	Reference(s)
A. The Sung Valley intrusion				
1	Perovskite from ijolite; SV10	<i>In situ</i> U-Pb SIMS	104.0±1.3	This study
2	Perovskite from dunite; SV31	<i>In situ</i> U-Pb SIMS	109.1±1.6	This study
3	Perovskite from uncomphagrite; SV33	<i>In situ</i> U-Pb SIMS	101.7±3.6	This study
4	Zircon from nepheline syenite; SV52A	<i>In situ</i> U-Pb SIMS	106.8±1.5	This study
5	Perovskite from ijolite; SV58	U-Pb TIMS	115.1±5.1	Srivastava et al. (2005)
6	Whole rock pyroxenite and phlogopite from carbonatite	Ar-Ar	107.2±0.8	Ray et al. (1999)
7	Whole rock carbonatite and pyroxenite, and phlogopite from carbonatite	Rb-Sr	106±11	Ray et al. (2000)
B. The Jasra intrusion				
1	Zircon from syenite; JS5S	<i>In situ</i> U-Pb SIMS	106.8±0.8	This study

2	Perovskite from clinopyroxenite; JS15P	<i>In situ</i> U-Pb SIMS	101.6±1.2	This study
3	Zircon and baddeleyite from syenite; JS5S	U-Pb TIMS	105.2±0.5	Heaman et al. (2002)

Table 3 Sr isotope composition of different minerals/ and bulk-rocks of Sung Valley and Jasra intrusions, Shillong Plateau, NE India.

	Mineral/Rock/Sample Number	$^{87}\text{Rb}/^{86}\text{Sr}$	$^{87}\text{Sr}/^{86}\text{Sr}$	2σ	$^{87}\text{Sr}/^{86}\text{Sr}_{\text{0}}$	$\varepsilon_{\text{Sr}}(\text{t})$	2σ	Age (Ma)	$^{87}\text{Sr}/^{86}\text{Sr}(\text{i})$	$\varepsilon_{\text{Sr}}(\text{i})$	References
Sung Valley intrusion											
1	Ap; clinopyroxenite; SV7	0.00008	0.71080	41	0.71080	91.2	0.58	105	0.71080	91.2	This study
2	Prv; ijolite; SV10	0.00019	0.70956	18	0.70960	73.6	0.26	104	0.70956	73.6	This study
3	Ap; ijolite; SV10	0.00006	0.70950	10	0.70950	72.7	0.14	104	0.70950	72.7	This study
4	Ap; nph syenite; SV25	0.00023	0.71034	6	0.71030	84.7	0.06	105	0.71034	84.7	This study
5	Prv; dunite; SV31	0.00018	0.70479	10	0.70480	5.9	0.14	109	0.70479	5.9	This study
6	Prv; uncomh.; SV33	0.00037	0.70660	420	0.70660	31.6	0.60	101.7	0.70660	31.5	This study
7	Ap; uncomh.; SV33	0.00014	0.70576	7	0.70580	19.6	0.01	101.7	0.70576	19.6	This study
8	Ap; nph syenite; SV52A	0.00003	0.70849	3	0.70850	58.4	0.04	106.8	0.70849	58.4	This study
9	Ap; carbonatite; SV73	0.00003	0.70474	2	0.70470	5.2	0.03	105	0.70474	5.2	This study
10	Cal; carbonatite; SV73	0.00001	0.70472	4	0.70470	4.9	0.06	105	0.70472	4.9	This study
11	Ap; ijolite; SV83	0.00006	0.70756	3	0.70760	45.2	0.04	105	0.70756	45.2	This study
12	WR; ijolite; SV14	0.11290	0.70585	11	0.70570	18.5	0.16	105	0.70568	18.5	1
13	WR; nph syenite; SV25	0.55420	0.71120	12	0.71040	85.1	0.17	105	0.71037	85.1	1
14	WR; ijolite; SV46	0.09243	0.70903	11	0.70890	64.1	0.16	105	0.70889	64.1	1
15	WR; carbonatite; SV49	0.00239	0.70483	20	0.70480	6.4	0.28	107.2	0.70483	6.5	1
16	WR; carbonatite; SV54	0.00127	0.70487	6	0.70490	7.0	0.09	107.2	0.70487	7.1	1
17	WR; carbonatite; GC1162	0.00002	0.70476	-	0.70480	5.4	-	107.2	0.70476	5.5	2
18	WR; carbonatite; GC1163	0.00009	0.70471	-	0.70470	4.7	-	107.2	0.70471	4.8	2
19	WR; carbonatite; GC1164	0.00004	0.70476	-	0.70480	5.4	-	107.2	0.70476	5.5	2
20	WR; carbonatite; GC1165	0.00054	0.70483	-	0.70480	6.4	-	107.2	0.70483	6.5	2
21	WR; carbonatite; GC1166	0.00049	0.70474	-	0.70470	5.2	-	107.2	0.70474	5.2	2
22	WR; carbonatite; S-102	0	0.70456	-	0.70460	2.6	-	107.2	0.70456	2.6	3
23	WR; carbonatite; S-111	0	0.70447	-	0.70450	1.3	-	107.2	0.70447	1.4	3
24	WR; carbonatite; S-114	0	0.70443	-	0.70440	0.8	-	107.2	0.70443	0.8	3
25	WR; carbonatite; S-115	0	0.70442	-	0.70440	0.6	-	107.2	0.70442	0.7	3
26	WR; uncomh; S-24	0.01000	0.70566	-	0.70570	18.0	-	105	0.70565	18.0	3
27	WR; uncomh; S-28	0.01000	0.70562	-	0.70560	17.4	-	105	0.70561	17.4	3
28	WR; clinopyroxenite; S-15	0.05000	0.70668	-	0.70660	31.6	-	105	0.70660	31.6	3
29	WR; clinopyroxenite; S-69	0.05000	0.70571	-	0.70560	17.9	-	105	0.70564	17.9	3
30	WR; syenite; S-8	0.58000	0.71165	-	0.71080	91.0	-	105	0.71078	91.0	3
31	WR; syenite; S-34	0.68000	0.71159	-	0.71060	88.0	-	105	0.71058	88.0	3
32	WR; syenite; S-35	0.44000	0.71113	-	0.71050	86.6	-	105	0.71047	86.6	3

33	WR; syenite; S-46	0.37000	0.71090	-	0.71040	84.8	-	105	0.71035	84.8	3
34	WR; syenite; S-65	0.46000	0.70906	-	0.70840	56.8	-	105	0.70837	56.7	3
Jasra intrusion											
1	Ap; essexite; JS2	0.00006	0.70732	2	0.70730	41.8	0.03	105	0.70732	41.8	This study
2	Ap; nph monzodiorite; JS5G	0.00006	0.70731	3	0.70730	41.6	0.04	105	0.70731	41.6	This study
3	Ap; syenite; JS5S	0.00011	0.70769	3	0.70770	47.0	0.04	106.8	0.70769	47.1	This study
4	Prv; clinopyroxenite; JS15P	0.00005	0.70684	3	0.70680	35.0	0.04	101.6	0.70684	34.9	This study
5	Ap; clinopyroxenite; JS15P	0.00001	0.70678	2	0.70680	34.1	0.03	101.6	0.70678	34.1	This study
6	Ap; clinopyroxenite; JS16	0.00017	0.70804	3	0.70800	52.0	0.04	105	0.70804	52.0	This study
7	Ap; ol monzodiorite; JS34	0.00033	0.70908	4	0.70910	66.8	0.06	105	0.70908	66.8	This study
8	Ap; shonkinit; JS39	0.00014	0.70720	3	0.70720	40.1	0.04	105	0.70720	40.1	This study
9	Ap; amp monzodiorite; JS42	0.00013	0.70778	2	0.70780	48.3	0.03	105	0.70778	48.3	This study
10	WR; syenite; JS5S	0.19600	0.70795	10	0.70770	46.6	0.14	106.8	0.70765	46.5	4
11	WR; nph syenite; JS15S	0.08438	0.70706	10	0.70690	36.3	0.14	105	0.70693	36.3	4
12	WR; clinopyroxenite; JS22	0.03481	0.70658	10	0.70650	30.5	0.14	105	0.70652	30.5	4
13	WR; ol monzodiorite; JS34	0.06885	0.70899	13	0.70890	64.1	0.18	105	0.70889	64.1	4
14	WR; clinopyroxenite; JS37	0.05542	0.70676	11	0.70670	32.6	0.16	105	0.70667	32.6	4

Epsilon Sr [$\epsilon_{\text{Sr(i)}}$] values are calculated using present-day ratios of $^{87}\text{Sr}/^{86}\text{Sr}=0.7045$ (DePaolo, 1988) and $^{87}\text{Rb}/^{86}\text{Sr}=0.0827$ (DePaolo, 1988) for Bulk Silicate Earth (BSE).

Ap: Apatite; Prv: Perovskite; Cal: Calcite; uncomphag: Uncompahgrite; nph: Nepheline; ol: Olivine; amp: Amphibole; WR: whole-rock.

References: 1. Srivastava et al. (2005); 2. Veena et al. (1998); 3. Ghatak and Basu (2013); 4. Srivastava and Sinha (2007).

Table 4 Nd isotope composition of minerals/ and bulk-rocks of Sung Valley and Jasra intrusions, Shillong Plateau, NE India.

	Mineral/Rock/Sample Number	$^{147}\text{Sm}/^{144}\text{Nd}$	$^{143}\text{Nd}/^{144}\text{Nd}$	2σ	$\epsilon_{\text{Nd(t)}}$	2σ	Age (Ma)	$^{143}\text{Nd}/^{144}\text{Nd (i)}$	$\epsilon_{\text{Nd(i)}}$	T DM	Reference
Sung Valley intrusion											
1	Ap; pyroxenite; SV7	0.1086	0.512083	17	-9.66	0.34	105	0.512008	-9.65	1.18	This study
2	Prv; ijolite; SV10	0.0867	0.512421	10	-2.77	0.2	105	0.512361	-2.76	0.68	This study
3	Ap; ijolite; SV10	0.0849	0.512443	10	-2.31	0.19	105	0.512385	-2.31	0.65	This study
4	Ap; nph syenite; SV25	0.0875	0.512007	24	10.88	0.52	105	0.511947	10.85	1.09	This study
5	Prv; dunite; SV31	0.0634	0.512579	12	0.65	0.23	109	0.512534	0.70	0.45	This study
6	Prv; uncomh.; SV33	0.0634	0.512579	12	0.65	0.23	101.7	0.512537	0.58	0.45	This study
7	Ap; nph syenite; SV52A	0.0858	0.512363	18	-3.88	0.36	106.8	0.512303	-3.85	0.73	This study
8	Bdy; carbonatite; SV73	0.0833	0.512573	23	0.23	0.47	105	0.512516	0.25	0.51	This study
9	Ap; carbonatite; SV73	0.1032	0.512618	13	0.91	0.27	105	0.512547	0.86	0.54	This study
10	WR; ijolite; SV14	0.1263	0.512535	15	-1.07	0.29	105	0.512448	-1.07	0.76	1
11	WR; nph syenite; SV24A	0.1161	0.511925	9	12.83	0.18	105	0.511845	12.83	1.44	1

12	WR; nph syenite; SV25	0.1111	0.512014	7	-11.02	0.14	105	0.511938	-11.03	1.28	1
13	WR; ijolite; SV46	0.0984	0.512371	5	-3.89	0.1	105	0.512303	-3.89	0.79	1
14	WR; carbonatite; SV49	0.1029	0.512611	7	0.73	0.14	107.2	0.512539	0.76	0.54	1
15	WR; carbonatite; SV54	0.1018	0.512611	11	0.75	0.21	107.2	0.512540	0.77	0.54	1
16	WR; carbonatite; GC1162	0.1035	0.51266	-	1.68	-	107.2	0.512587	1.70	0.49	2
17	WR; carbonatite; GC1163	0.0994	0.51264	-	1.34	-	107.2	0.512570	1.37	0.50	2
18	WR; carbonatite; GC1164	0.0994	0.51265	-	1.54	-	107.2	0.512580	1.57	0.49	2
19	WR; carbonatite; GC1165	0.0815	0.51265	-	1.78	-	107.2	0.512593	1.81	0.43	2
20	WR; carbonatite; GC1166	0.0999	0.51264	-	1.34	-	107.2	0.512570	1.36	0.50	2
21	WR; carbonatite; S- 102	0.11	0.51262	-	0.81	-	107.2	0.512543	0.84	0.56	3
22	WR; carbonatite; S- 111	0.1	0.51265	-	1.53	-	107.2	0.512580	1.56	0.49	3
23	WR; carbonatite; S- 114	0.11	0.51262	-	0.81	-	107.2	0.512543	0.84	0.56	3
24	WR; carbonatite; S- 115	0.11	0.51265	-	1.4	-	107.2	0.512573	1.42	0.53	3
25	WR; uncomh; S-24	0.13	0.51254	-	-1.02	-	105	0.512451	-1.02	0.78	3
26	WR; uncomh; S-28	0.11	0.51262	-	0.81	-	105	0.512544	0.81	0.56	3
27	WR; pyroxenite; S-15	0.12	0.51251	-	-1.47	-	105	0.512428	-1.47	0.75	3
28	WR; pyroxenite; S-69	0.11	0.51254	-	-0.75	-	105	0.512464	-0.75	0.66	3
29	WR; syenite; S-8	0.12	0.51197	-	-12.01	-	105	0.511888	-12.01	1.43	3
30	WR; syenite; S-34	0.13	0.51192	-	-13.12	-	105	0.511831	-13.12	1.63	3
31	WR; syenite; S-35	0.12	0.51205	-	-10.45	-	105	0.511968	-10.45	1.33	3
32	WR; syenite; S-46	0.12	0.51203	-	-10.84	-	105	0.511948	-10.84	1.36	3
33	WR; syenite; S-65	0.13	0.51249	-	-1.99	-	105	0.512401	-1.99	0.85	3
Jasra intrusion											
1	Ap; essexite; JS2	0.0908	0.512496	13	-1.34	0.25	105	0.512434	-1.35	0.62	This stu
2	Ap; nph monzodiorite; JS5G	0.0862	0.512501	9	-1.19	0.18	105	0.512442	-1.19	0.59	This stu
3	Ap; syenite; JS5S	0.0875	0.512513	8	-0.98	0.15	106.8	0.512452	-0.95	0.59	This stu
4	Prv; pyroxenite; JS15P	0.0879	0.512517	6	-0.87	0.24	101.6	0.512459	-0.95	0.58	This stu
5	Ttn; pyroxenite; JS15P	0.1331	0.51253	27	-1.66	0.39	101.6	0.512442	-1.28	0.81	This stu
6	Ap; pyroxenite; JS15P	0.0962	0.512483	10	-1.68	0.2	101.6	0.512419	-1.72	0.65	This stu
7	Ap; clinopyroxenite; JS16	0.0793	0.512347	10	-4.11	0.19	105	0.512293	-4.10	0.71	This stu
8	Ap; ol monzodiorite; JS34	0.088	0.512428	13	-2.69	0.25	105	0.512368	-2.64	0.67	This stu
9	Ttn; shonkinite; JS39	0.133	0.512507	29	-1.65	0.53	105	0.512416	-1.70	0.85	This stu
10	Ap; shonkinite; JS39	0.0936	0.512439	16	-2.48	0.31	105	0.512375	-2.50	0.69	This stu
11	Ap; amp monzodiorite; JS42	0.0925	0.512496	8	-1.35	0.15	105	0.512432	-1.37	0.62	This stu
12	WR; syenite; JS5S	0.09221	0.51245	11	-2.27	0.22	106.8	0.512386	-2.24	0.67	4
13	WR; nph syenite; JS15S	0.1103	0.512334	6	-4.78	0.12	105	0.512258	-4.77	0.90	4
14	WR; clinopyroxenite; JS22	0.08677	0.512487	6	-1.47	0.12	105	0.512427	-1.47	0.61	4

15	WR; ol monzodiorite; JS34	0.11623	0.512397	17	-3.62	0.33	105	0.512317	-3.62	0.87		4
16	WR; clinopyroxenite; JS37	0.09828	0.512532	11	-0.75	0.22	105	0.512464	-0.75	0.61		4

The epsilon Nd [$\epsilon_{\text{Nd}}(\text{i})$] values were calculated using present-day ratios $^{147}\text{Sm}/^{144}\text{Nd}=0.1967$ (Jacobsen and Wasserburg, 1980) for CHondritic Uniform Reservoir (CHUR).

Abbreviations: Ap: Apatite; Prv: Perovskite; Bdy: Baddeleyite; Ttn: Titanite; uncomphg: Uncomphgrite; neph: Nepheline; ol: Olivine; amp: Amphibole; WR: whole-rock.

References: 1. Srivastava et al. (2005); 2. Veena et al. (1998); 3. Ghatak and Basu (2013); 4. Srivastava and Sinha (2007).

Table 5 Hf isotope data of different minerals of Sung Valley and Jasra intrusions, Shillong Plateau, NE India

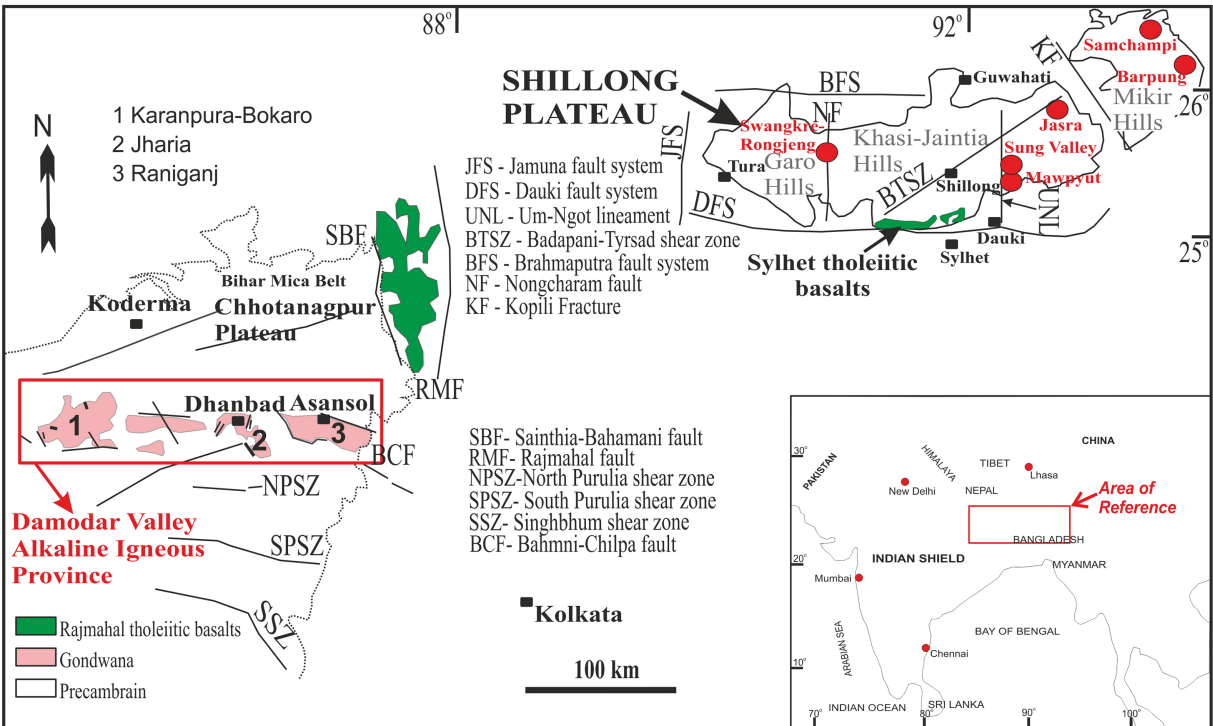
	Mineral/Rock/Sample Number	$^{176}\text{Lu}/^{177}\text{Hf}$	$^{176}\text{Hf}/^{177}\text{Hf}$	2σ	$\epsilon_{\text{Hf}}(t)$	2σ	Age (Ga)	$^{176}\text{Hf}/^{177}\text{Hf}$	$\epsilon_{\text{Hf}}(\text{i})$	T DM Hf	Reference
Sung Valley intrusion											
1	Zrn; neph syenite; SV52A	0.00051	0.282562	12	-5.16	2	0.01068	0.282562	-7.43	0.96	This study
2	Bdy; carbonatite; SV73	0.00007	0.282815	8	3.82	0.28	0.01050	0.282815	1.52	0.61	This study
Jasra intrusion											
1	Bdy; neph monzodiorite; JS5G	0.000122	0.282702	6	-0.18	0.21	0.01050	0.282702	-2.48	0.76	This study
2	Bdy; syenite; JS5S	0.00008	0.282668	16	-1.38	0.57	0.01068	0.282668	-3.68	0.81	This study
3	Zrn; syenite; JS5S	0.00098	0.282673	10	-1.27	0.35	0.01050	0.282673	-3.50	0.82	This study

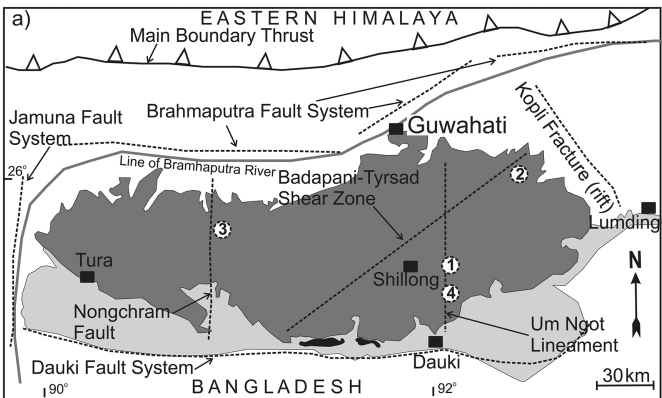
The epsilon Hf [$\epsilon_{\text{Hf}}(\text{i})$] values were calculated using decay constant (λ) of 1.865×10^{-11} (Scherer et al., 2006) and depleted mantle values: $^{176}\text{Lu}/^{177}\text{Hf}=0.0384$ and $^{176}\text{Hf}/^{177}\text{Hf}=0.28325$ (Blichert-Toft and Albarede, 1997).

Abbreviations: Zrn: Zircon; Bdy: Baddeleyite; neph: nepheline.

Highlights

- New *in-situ* U–Pb ages are 102–109 Ma for the Sung Valley and Jasra intrusions
- Sung Valley carbonatite isotopes suggest a mantle source in metasomatized lithosphere
- Metasomatic event in the lithosphere took place in pre-Mesozoic times
- The Sr-Nd-Hf isotopes of silicate rocks indicates low-pressure crustal contamination





1

2

3

4

5

6

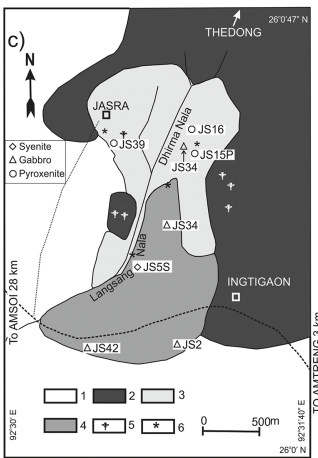
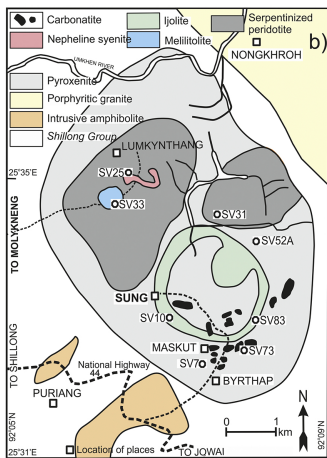


Figure 2

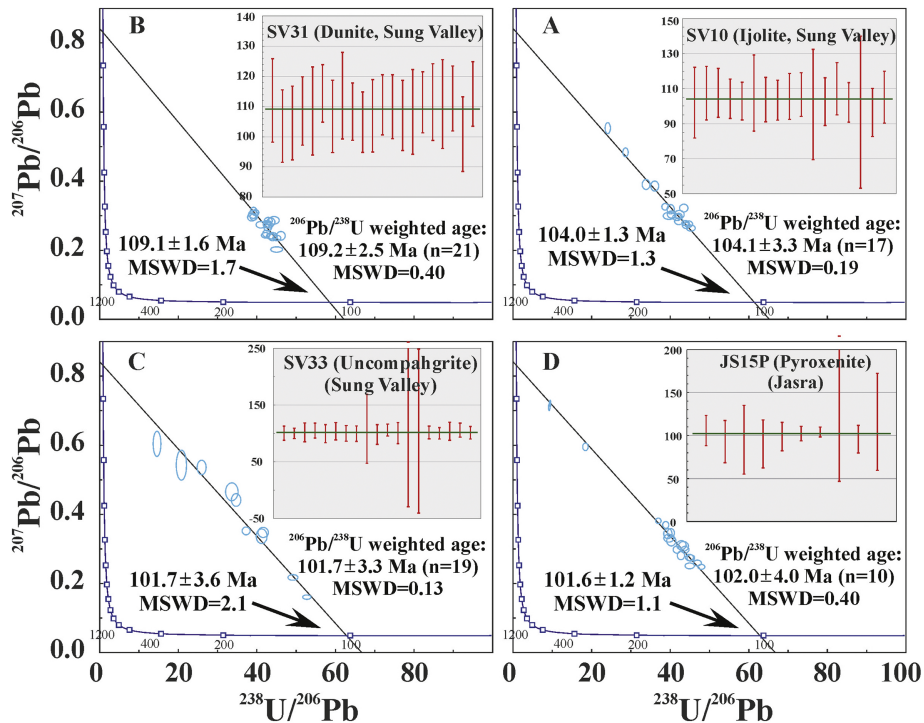


Figure 3

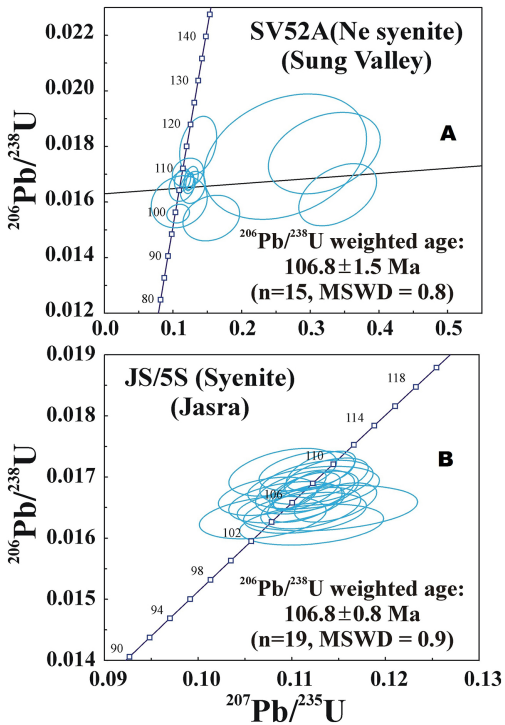


Figure 4

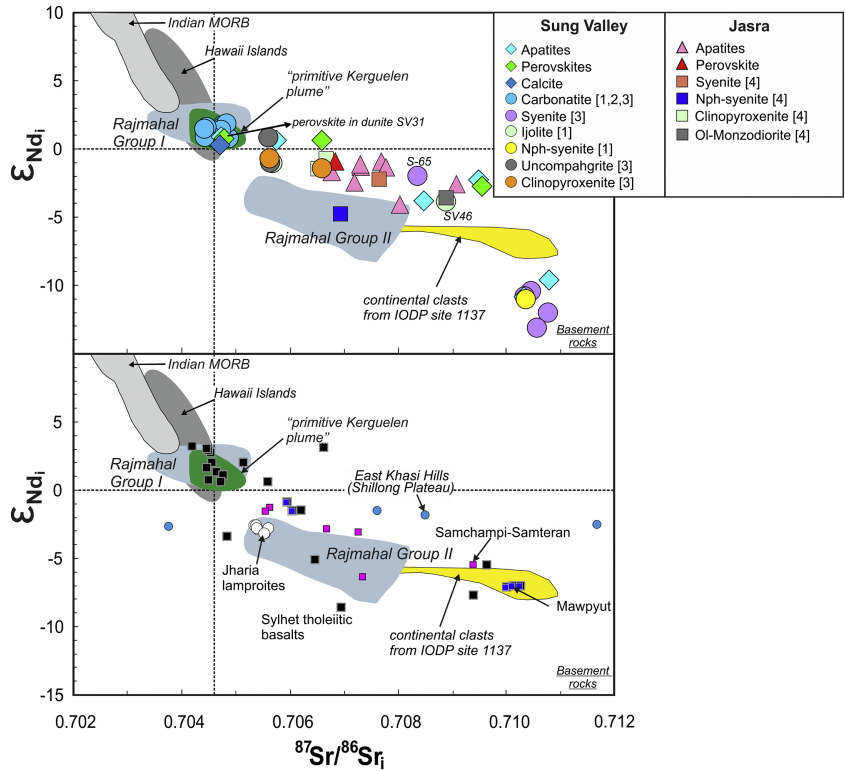


Figure 5

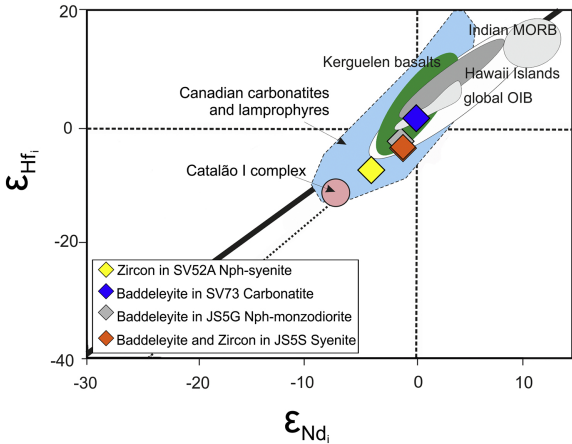


Figure 6

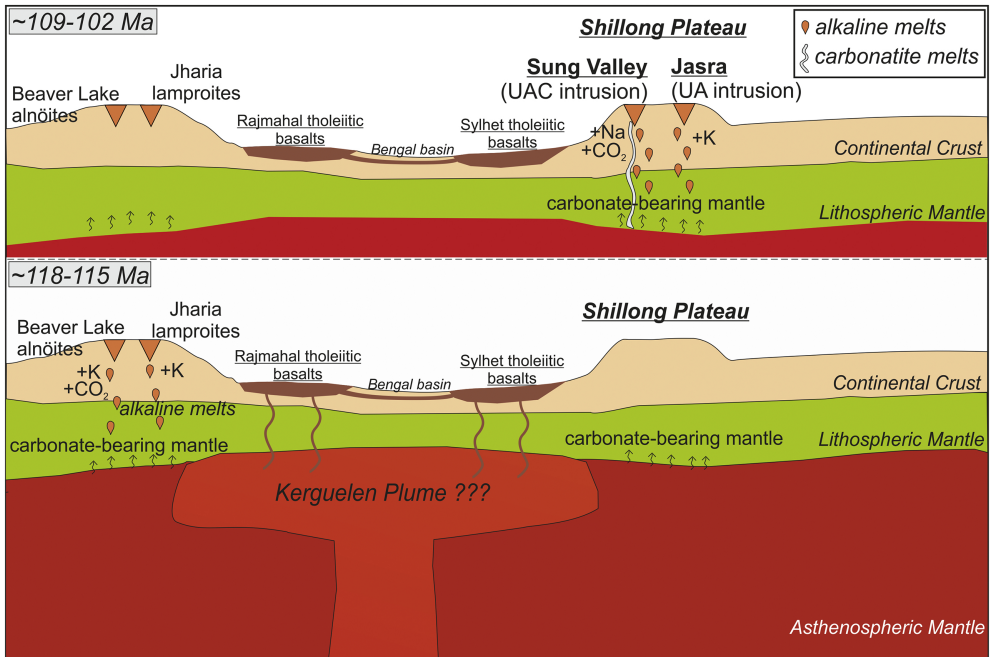


Figure 7

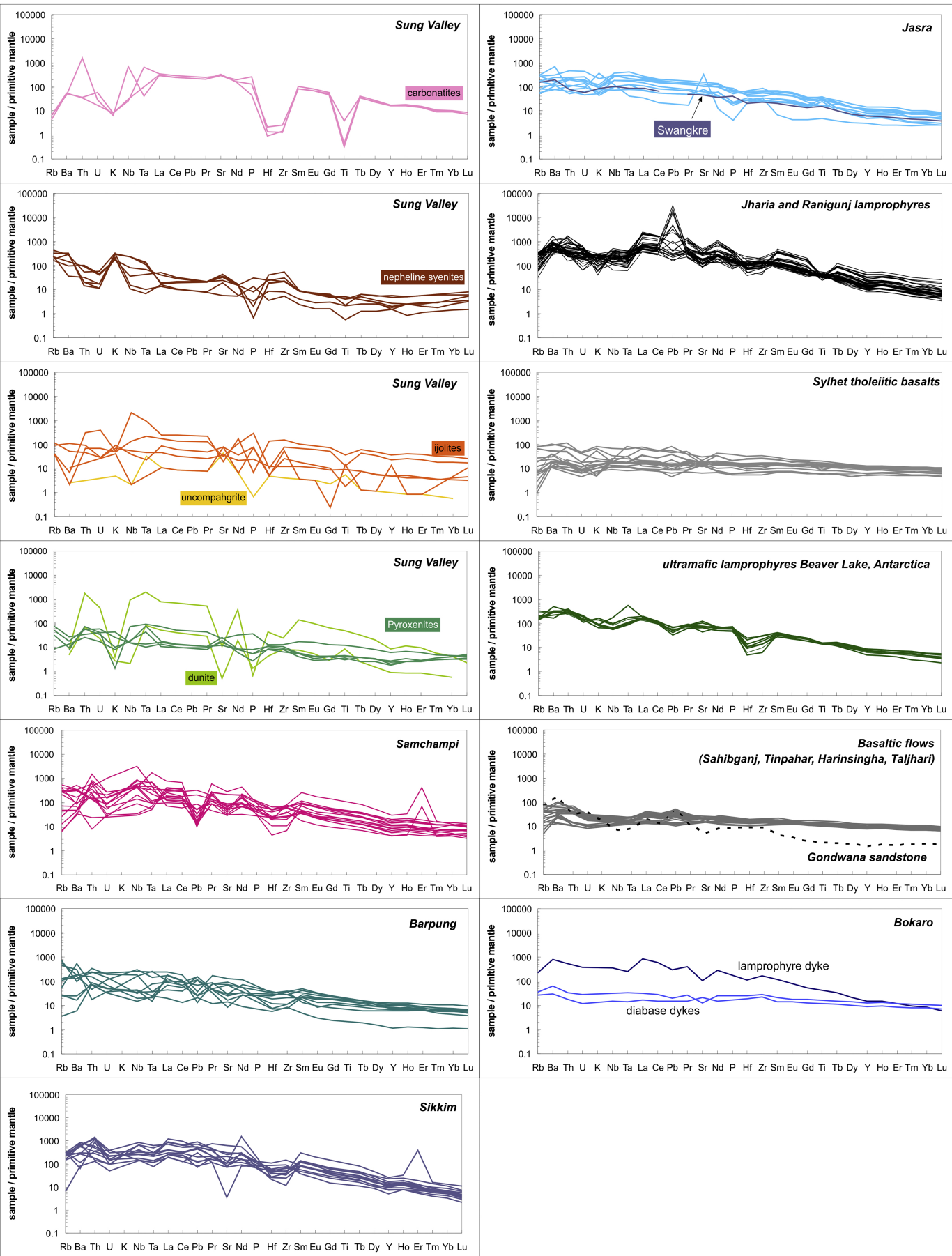


Figure 8